Antimalarial Benzimidazole Derivatives Incorporating Phenolic Mannich Base Side Chains inhibit Microtubule and Hemozoin formation: Structure-Activity Relationship and In Vivo Oral Efficacy Studies

Godwin Akpeko Dziwornu,[a] Dina Coertzen,[b] Meta Leshabane,[b] Constance M. Korkor,[a] Cleavon K. Cloete,[a] Mathew Njoroge,[c] Liezl Gibhard,[c] Nina Lawrence,[c] Janette Reader,[b] Mariëtte van der Watt,[b] Sergio Wittlin,[d,e] Lyn-Marie Birkholtz,[b] Kelly Chibale*[a,f,g]

[a]Department of Chemistry, University of Cape Town, Rondebosch 7701, South Africa

[b]Department of Biochemistry, Genetics and Microbiology, University of Pretoria Institute for Sustainable Malaria Control, University of Pretoria, Private Bag X20, Hatfield 0028, South Africa

[c]Drug Discovery and Development Centre (H3D), Division of Clinical Pharmacology, Department of Medicine, University of Cape Town, Observatory 7925, South Africa

[d]Swiss Tropical and Public Health Institute, Socinstrasse 57, Basel 4002, Switzerland

[e]University of Basel, Basel 4003, Switzerland

[f]Institute of Infectious Disease and Molecular Medicine, University of Cape Town, Rondebosch 7701, South Africa

[g]South African Medical Research Council Drug Discovery and Development Research Unit, University of Cape Town, Rondebosch 7701, South Africa

*Corresponding author: Email: kelly.chibale@uct.ac.za; Phone: +27-21-6502553

ABSTRACT

A novel series of antimalarial benzimidazole derivatives incorporating phenolic Mannich base side chains at the C2 position, which possess dual asexual blood and sexual stage activities is presented. Structure-activity relationship studies revealed that the 1-benzylbenzimidazole analogues possessed sub-micromolar asexual blood and sexual stage activities in contrast to the 1*H*-benzimidazole analogues, which were only active against asexual blood stage (ABS) parasites. Further, the former demonstrated microtubule inhibitory activity in ABS parasites but more significantly in stage II/III gametocytes. In addition to being bona fide inhibitors of hemozoin formation, the 1*H* benzimidazole analogues also showed inhibitory effects on microtubules. In vivo efficacy studies in *P. berghei*-infected mice revealed that frontrunner compound 41 exhibited high efficacy (98% reduction in parasitemia) when dosed orally at 4x50 mg/kg. Generally, the compounds were non-cytotoxic to mammalian cells.

KEYWORDS: antiplasmodium, antimalarial, gametocytes, benzimidazole, phenolic Mannich bases, hemozoin, microtubules

INTRODUCTION

Efforts in the fight against malaria saw a decline in incidence rates from 2010 to 2015, which have since plateaued out with sub-Saharan Africa still carrying the heaviest disease burden. Artemisinin-based combination therapy (ACT), the current first-line chemotherapy regimen for the treatment of malaria caused by *Plasmodium falciparum*, has been successful in most parts of the world although artemisinin resistance has been reported in Cambodia, Lao People's Democratic Republic, and Vietnam.[1] More recently, genetic markers of resistance to artemisinins, namely a validated mutation in the Pfkelch13 gene (K13 R561H), have been identified in Rwanda, which is an alarming sign for a possible evolution towards treatment failures as witnessed in South East Asia during the last 2 decades.[2] Apart from the artemisinin-based endoperoxides, current drugs belong mainly to the aminoquinoline, sulfonamides and amino alcohol chemical classes, which also have significant resistance rates, negating their use as monotherapies.[3]

Undoubtedly, there is a need for structurally differentiated novel antimalarials, regardless of mode of action, to overcome current and emerging drug resistance challenges.[4] Further, the advent and periodic optimization of target candidate and product profiles (TCPs and TPPs) for new malaria medicines has provided a more definitive roadmap for drug discovery efforts at an early stage that considers all stages of the parasite's lifecycle as potential druggable targets to combat and eradicate the disease.[5,6]

Complemented by its binding possibilities to a wide range of biological targets, the benzimidazole scaffold has been extensively explored in drug discovery. Several reviews and research articles have reported the diverse biological properties of benzimidazole derivatives.[7–10] Within the

context of malaria, the antimalarial properties of benzimidazole derivatives has been reported[11–17].

Like the benzimidazole substructure, the biological usefulness of Mannich bases is evident in some current drugs on the market including amodiaquine, the first Mannich base used to treat malaria. Notwithstanding its success as an antimalarial drug, rapid oxidative metabolism of the 4-aminophenol moiety of amodiaquine to an electrophilic 1,4-quinoneimine and aldehyde 1,4-quinoneimine metabolites, highly reactive to intracellular glutathione and other protein molecules, has been associated with hepatotoxicity and agranulocytosis.[18–20] Other antimalarial phenolic Mannich bases include WR-194,965, JPC-2997, and MK-4815, which is still in preclinical studies. (Figure 1).[21–23]

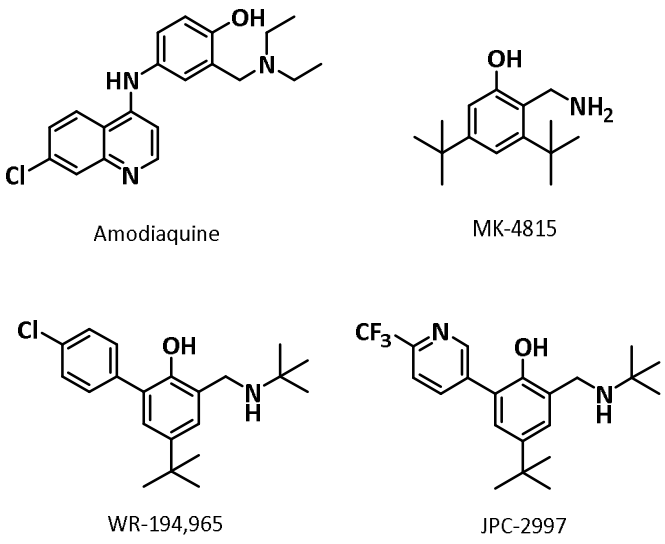

Figure 1: Examples of Antimalarial Mannich bases

The abovementioned presence of benzimidazole and phenolic Mannich base moieties in antimalarial agents provided a rational basis for attaching phenolic Mannich base side chains to a benzimidazole core. Two structure-activity relationship (SAR) studies were undertaken in the

present work (Figure 2). SAR 1 focused on exploring 2-, 3-, and 4-amino phenol Mannich bases at the C2 position of the benzimidazole core, along with investigating the contributions of *para*-substituted benzyl groups at the *N*1 position. The diethylaminomethylene Mannich base side chain was kept constant in SAR 1. Subsequently, SAR 2 was undertaken to optimize the frontrunner compound from SAR 1 by derivatizing the phenolic Mannich base while introducing fluoro- and chloro-substituents on the benzimidazole core.

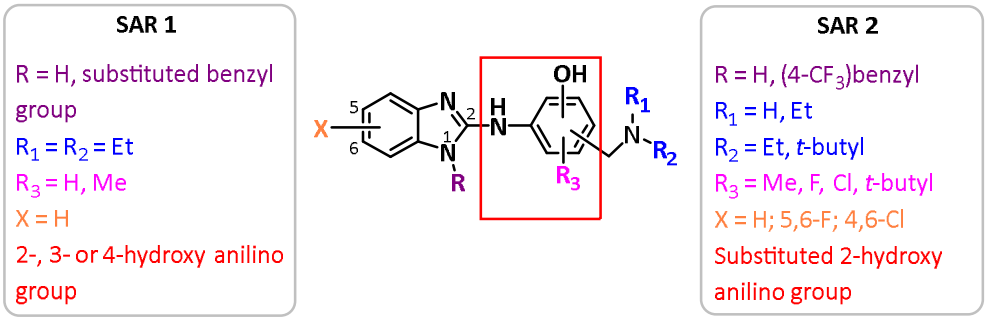

Figure 2: Summary of SAR exploration

RESULTS AND DISCUSSION

Chemistry: The synthesis of the target compounds is described in Scheme 1. Briefly, 2-chloro-1*H*-benzimidazole (1) was reacted with 4-cyanobenzyl bromide or 4-(trifluoromethyl)benzyl bromide in the presence of K_2CO_3 to obtain the respective substituted 1-benzyl-2-chlorobenzimidazole (2 and 3). Meanwhile, compounds 5 and 6 were synthesized *via* chlorination of 1,3-dihydro-2-oxo-benzimidazole intermediates I and II in the presence of phosphoryl oxychloride. Compound 7 was obtained from 5 as previously described above.

The phenolic Mannich bases (11a-m) were obtained as hydrochloride salts by first subjecting the respective amino phenols (8a-i) to an acetylation reaction with acetic anhydride in THF to protect the amino group as the acetamides (9a-i). These were then subjected to a Mannich condensation

reaction with formaldehyde in the presence of *N*,*N*-diethylamine or *N*-ethylamine or *N*-*tert*-butylamine in EtOH. Lastly, acid hydrolysis afforded the Mannich bases 11a-m. The target compounds 12-51 were finally synthesized *via* nucleophilic aromatic substitution of the 2-chloro benzimidazoles 1-7 with the phenolic Mannich bases 11a-m in the presence of KH_2PO_4 as base and *n*-BuOH as the solvent. Meanwhile, acid-cleavage of the *p*-methoxybenzyl (PMB) protecting group of intermediate III afforded 52.

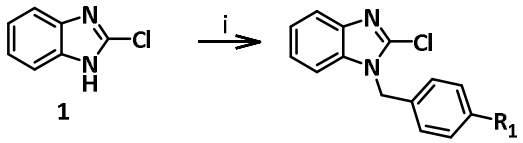

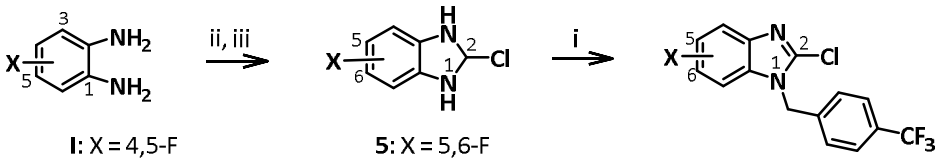

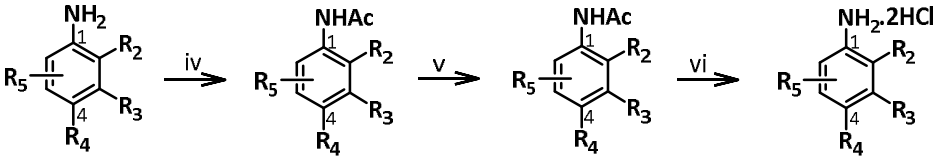

a: $R_2 = R_3 = R_5 = H$; $R_4 = OH$
b: $R_2 = R_4 = R_5 = H$; $R_3 = OH$
c: $R_2 = OH$; $R_3 = R_4 = R_5 = H$
d: $R_2 = OH$; $R_3 = R_4 = H$; R_5 = 5-Me
e: $R_2 = OH$; $R_3 = R_4 = H$; R_5 = 6-Me
f: $R_2 = OH$; $R_3 = R_4 = H$; R_5 = 5-Cl
g: $R_2 = OH$; $R_3 = R_5 = H$; R_4 = Cl
h: $R_2 = OH$; $R_3 = R_4 = H$; R_5 = 5-F
i: $R_2 = OH$; $R_3 = R_4 = H$; R_5 = 5-*t*-Bu

a: $R_2 = R_5 = H$; $R_3 = CH_2NEt_2$; $R_4 = OH$
b: $R_2 = R_5 = H$; $R_3 = OH$; $R_4 = CH_2NEt_2$
c: $R_2 = OH$; $R_3 = CH_2NEt_2$; $R_4 = R_5 = H$
d: $R_2 = OH$; $R_3 = CH_2NEt_2$; $R_4 = H$; R_5 = 5-Me
e: $R_2 = OH$; $R_3 = CH_2NEt_2$; $R_4 = H$; R_5 = 6-Me
f: $R_2 = OH$; $R_3 = CH_2NHEt$; $R_4 = H$; R_5 = 5-Me
g: $R_2 = OH$; $R_3 = CH_2NH(t\text{-Bu})$; $R_4 = H$; R_5 = 5-Me
h: $R_2 = OH$; $R_3 = CH_2NEt_2$; $R_4 = H$; R_5 = 5-Cl
i: $R_2 = OH$; $R_3 = CH_2NHEt$; $R_4 = H$; R_5 = 5-Cl
j: $R_2 = OH$; $R_3 = CH_2NH(t\text{-Bu})$; $R_4 = H$; R_5 = 5-Cl
k: $R_2 = OH$; $R_3 = CH_2NEt_2$; R_4 = Cl; $R_5 = H$
l: $R_2 = OH$; $R_3 = CH_2NEt_2$; $R_4 = H$; R_5 = 5-F
m: $R_2 = OH$; $R_3 = CH_2NH(t\text{-Bu})$; $R_4 = H$; R_5 = 5-*t*-Bu

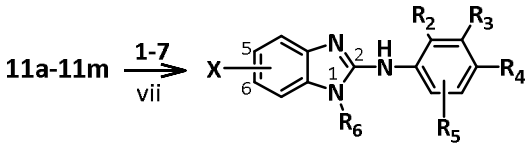

R_2 = H; OH
R_3 = OH; CH_2NEt_2; CH_2NHEt; $CH_2NH(t\text{-Bu})$
R_4 = H; OH; Cl; CH_2NEt_2
R_5 = H; 5-Me; 6-Me; 5-Cl; 5-F; 5-*t*-Bu
R_6 = H; (4-CN)$C_6H_4CH_2$; (4-CF_3)$C_6H_4CH_2$; (4-F)$C_6H_4CH_2$
X = H; 5,6-F; 4,6-Cl

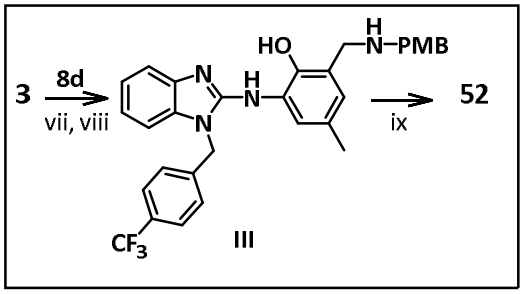

Scheme 1: Reagents and reaction conditions: (i) appropriate benzyl bromide, K_2CO_3, CH_3CN, 75 °C, 2 h; (ii) appropriate 1,2-diaminobenzene, urea, THF, 130 °C, MW, 30 min.; (iii) $POCl_3$, 130 °C, 3 h; (iv) acetic anhydride, THF, 60 °C, 1 h (for 9a-i); (v) appropriate amine, HCHO, EtOH, 85 °C, 2 h; (vi) 6N HCl, 100 °C, 2 h (for 11a-m); (vii) KH_2PO_4,

n-BuOH, 100 ºC, 8 h (for 12-51); (viii) *p*-methoxybenzyl amine, HCHO, EtOH, 85 ºC, 16 h (for III); (ix) TFA, DCM, 25 ºC, 48 h (for 52).

Multi-stage antiplasmodium activity: The synthesized benzimidazole analogues were evaluated for their *in vitro* multi-stage antiplasmodium activity against the asexual blood stage (ABS) drug sensitive (NF54) and multi-drug resistant (K1) strains, and early- (stage II/III) and late-stage (stage IV/V) gametocytes of *P. falciparum* (Table 1). Regarding SAR 1 exploration, based on the Mannich base used, the 5-methyl-3-((*N*,*N*-diethylamino)methyl)-2-hydroxy aniline (R' = D, Table 1) showed superior activity(IC_{50} *Pf*NF54/K1 = [0.19 – 0.65]/[0.06 – 0.46] µM) against both strains, followed by its parent 3-((*N*,*N*-diethylamino)methyl)-2-hydroxy aniline (R' = C; IC_{50} *Pf*NF54/K1 = [0.36 – 1.00]/[0.13 – 0.77] µM). For example, among the synthesized 1*H*-benzimidazole series, compounds 14 and 15 displayed sub-micromolar potency against both NF54 and K1 strains with IC_{50} *Pf*NF54/K1 = 0.56/0.77 µM and IC_{50} *Pf*NF54/K1 = 0.23/0.42 µM, respectively, with no evidence of cross-resistance (RI values 1.38 and 1.83). Compounds 12 and 16 showed good activity (IC_{50} <1 µM) against the NF54 strain but the latter displayed moderate activity (IC_{50} = 1.62 µM) against K1 parasites while 12 lost activity (RI value 9.09). Compound 13 was the least active of the 1*H*-benzimidazole analogues, showing largest cross-resistance formation (IC_{50} *Pf*NF54/K1 = 1.88/>10 µM).

All analogues belonging to the *N*-benzyl benzimidazole series displayed sub-micromolar activity against the NF54 strain, except compounds 26 (IC_{50} = 2.88 µM) and 31 (IC_{50} = 2.27 µM) (Table 1). Generally, the 1-((4-trifluoromethyl)benzyl) (22 – 26, IC_{50} *Pf*NF54/K1 = [0.19 – 0.47]/[0.06 – 1.69] µM) displayed superior activity to the 1-(4-fluorobenzyl)benzimidazole analogues (27 – 31, IC_{50} *Pf*NF54/K1 = [0.36 – 0.68]/[0.18 – 1.95] µM) and the 1-(4-cyanobenzyl)benzimidazole analogues

(17 – 21, IC_{50} *Pf*NF54/K1 = [0.37 – 0.87]/[0.46 – 1.97] µM). All *N*-benzyl analogues of the 3-((*N*,*N*-diethylamino)methyl)-4-hydroxy aniline Mannich base were the least active in each series against the K1 strain (IC_{50} *Pf*K1 = 1.69 – 1.97 µM, Table 1). Consequently, compound 25, which bears 1-((4-trifluoromethyl)benzyl) benzimidazole incorporating the 5-methyl-3-((*N*,*N*-diethylamino)methyl)-2-hydroxy aniline, was the most potent against the ABS parasites (IC_{50} *Pf*NF54/K1 = 0.19/0.06 µM), with notable activity against the K1 strain, with no cross-resistance formation.

Subsequent SAR 2 studies focused on compound 25 as the frontrunner. Synthesized compounds for SAR 2 studies maintained sub-micromolar activity against both strains, except compound 38 (IC_{50} *Pf*NF54/K1 = 1.84/0.38 µM, Table 2). From a SAR perspective, compounds containing the diethylaminomethylene Mannich base side chain were more active than those containing the corresponding monoethylaminomethylene and *t*-butylaminomethylene Mannich base side chains. This is specifically evident in the activities of 25 (IC_{50} *Pf*NF54/K1 = 0.19/0.06 µM), 32 (IC_{50} *Pf*NF54/K1 = 0.78/0.30 µM) and 33 (IC_{50} *Pf*NF54/K1 = 0.40/0.23 µM), and 34 (IC_{50} *Pf*NF54/K1 = 0.15/0.05 µM), 35 (IC_{50} *Pf*NF54/K1 = 0.28/0.11 µM) and 36 (IC_{50} *Pf*NF54/K1 = 0.28/0.06 µM), respectively. The activity of 34 (IC_{50} *Pf*NF54/K1 = 0.15/0.05 µM) was comparable to 25 (IC_{50} *Pf*NF54/K1 = 0.19/0.06 µM), suggesting that the methyl group can be replaced with a chloro group on the phenol moiety. Similarly, potency was maintained with the fluoro substituent, as evident in 37 (IC_{50} *Pf*NF54/K1 = 0.17/0.19 µM), although a decrease in activity against the K1 strain was observed. On the contrary, the loss in activity of 38 (IC_{50} *Pf*NF54/K1 = 1.84/0.38 µM), a positional isomer of 34 (IC_{50} *Pf*NF54/K1 = 0.15/0.05 µM), suggests that the C5' position of the phenol moiety is optimal for activity. Furthermore, a comparison of the activities of 39 (IC_{50}

*Pf*NF54/K1 = 0.26/0.13 µM) and 40 (IC_{50} *Pf*NF54/K1 = 0.25/0.15 µM) to 32 (IC_{50} *Pf*NF54/K1 = 0.78/0.30 µM) and 33 (IC_{50} *Pf*NF54/K1 = 0.40/0.23 µM), respectively, seem to suggest that fluoro substitution on the benzimidazole core scaffold potentiates activity. The 1-benzylbenzimidazole analogues 32 - 42 maintained better potency against the K1 strain than the NF54 strain of *P. falciparum*, as observed for their SAR 1 congeners above.

The 1*H*-benzimidazole analogues 43 - 51 exhibited similar SAR trends as described for the 1-benzylbenzimidazole analogues, showing comparable sub-micromolar IC_{50} values (*Pf*NF54/K1 = [0.15 – 0.30]/[0.25 – 0.88] µM, Table 2). This seems to suggest that the benzyl moiety does not significantly contribute to antiplasmodium activity. It is also evident from this series of compounds that the C5' *tert*-butyl group, as in 46 and 50, makes a positive contribution to activity albeit has the drawback of increasing lipophilicity. In contrast to the 1-benzylbenzimidazole analogues, the SAR 2 1*H*-benzimidazole derivatives, like their SAR 1 congeners, were more potent against the NF54 than the K1 strain of *P. falciparum* with an average RI of 2.75.

Table 1: *In vitro* antiplasmodium activity against sensitive (NF54) and multidrug-resistant strains (K1) and cytotoxicity of SAR 1 compounds

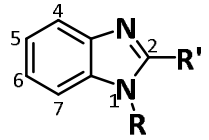

R' =

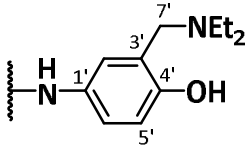

A

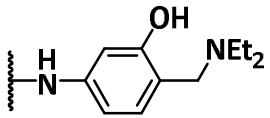

B

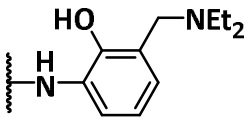

C

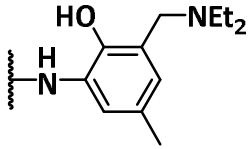

D

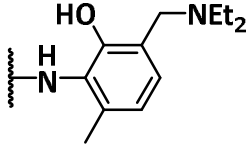

E

Compound	R	R[I]	ABS,[a] IC_{50} (µM)			Gametocytes, % inhibition (5 µM/1 µM)			Cytotoxicity IC_{50} (µM)	
			*Pf*NF54	*Pf*K1	RI[b]	EG[c]	IC_{50} (µM)[d]	LG[e]	CHO[f]	SI[g]
12	H	A	0.80	7.27	9.09	9/30		28/0	>50	>62
13	H	B	1.88	>10	>5.32				>50	>26
14	H	C	0.56	0.77	1.38	0/3		34/0	>50	>89
15	H	D	0.23	0.42	1.83	44/1		37/34	>50	>217
16	H	E	0.86	1.62	1.88	32/3		31/34	>50	>58
17	(4-CN)$C_6H_4CH_2$	A	0.47	1.97	4.19	23/20		35/9	>50	>106
18	(4-CN)$C_6H_4CH_2$	B	0.37	0.76	2.05	44/38		21/4	39.04	105.51
19	(4-CN)$C_6H_4CH_2$	C	1.00	0.66	0.66	69/47		43/19	>50	>50
20	(4-CN)$C_6H_4CH_2$	D	0.65	0.46	0.71	98/39		52/15	14.19	21.83
21	(4-CN)$C_6H_4CH_2$	E	0.87	0.83	0.95	96/19		22/0	>50	>57
22	(4-CF_3)$C_6H_4CH_2$	A	0.39	1.69	4.33	48/34		45/31	17.50	44.87
23	(4-CF_3)$C_6H_4CH_2$	B	0.47	0.87	1.85	41/36		24/2	41.50	88.29
24	(4-CF_3)$C_6H_4CH_2$	C	0.44	0.13	0.30	93/71	1.45	56/35	>50	>113

25	(4-CF_3)$C_6H_4CH_2$	D	0.19	0.06	0.32	97/91	0.11	62/41	29.31	154.26
26	(4-CF_3)$C_6H_4CH_2$	E	2.88	0.94	0.33	90/18		43/1	33.88	11.76
27	(4-F)$C_6H_4CH_2$	A	0.68	1.95	2.87	59/33		39/22	11.99	17.63
28	(4-F)$C_6H_4CH_2$	B	0.64	1.28	2.00	15/12		36/29	45.79	71.54
29	(4-F)$C_6H_4CH_2$	C	0.36	0.18	0.50	91/65	2.23	58/11	>50	>136
30	(4-F)$C_6H_4CH_2$	D	0.55	0.21	0.38	97/81	0.88	58/31	18.70	34.00
31	(4-F)$C_6H_4CH_2$	E	2.27	1.32	0.58	24/14		39/36	>50	>22
Chloroquine			0.01	0.42	42.00					
Emetine									0.02	
Methylene blue						93[h]	0.19	90[h]	0.14	

[a]ABS = Asexual Blood Stage, IC_{50}s represent mean from n values of ≥2 independent experiments; [b]RI = resistance index (ratio of IC_{50} [K1]: IC_{50} [NF54]), [c]EG = Early-stage gametocytes (stage I/III); [d]IC_{50}s against early gametocytes; [e]LG = Late-stage gametocytes (stage IV/V); [f]CHO = Chinese Hamster Ovarian cell line; [g]SI = selectivity index (ratio of IC_{50}[CHO]: IC_{50}[NF54]); [h]%Inhibition at 1 µM; Dual-point values were determined for one biological repeat (n=1), in technical triplicates. IC_{50} values are means from at least three independent biological repeats (n ≥ 3) performed in technical triplicates. Blank spaces = not tested

Table 2: *In vitro* antiplasmodium activity against sensitive (NF54) and multidrug-resistant strains (K1) and cytotoxicity of SAR 2 compounds

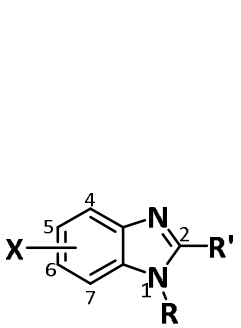

R'

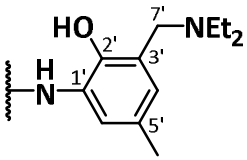

D

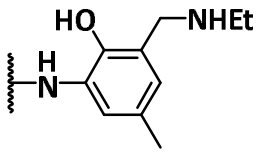

F

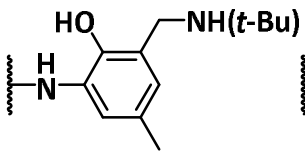

G

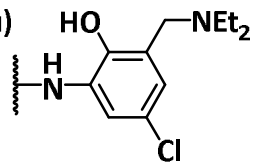

J

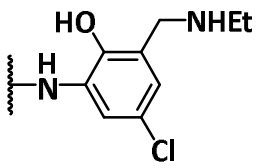

K

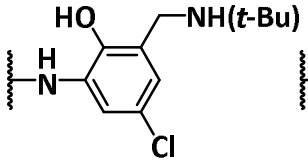

L

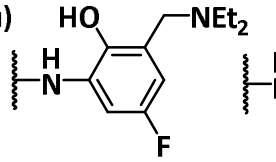

M

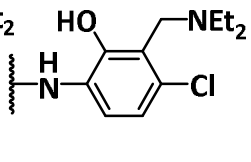

N

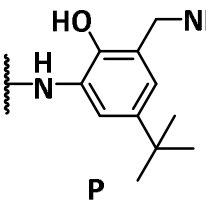

P

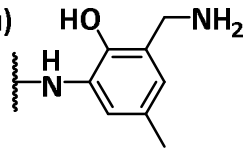

Q

Compound	X	R	R'	ABS,[a] IC_{50} (µM)			Gametocyte, % inhibition (5 µM/1 µM)				Cytotoxicity, IC_{50} (µM)	
				*Pf*NF54	*Pf*K1	RI[b]	EG	IC_{50} (µM)	LG	IC_{50} (µM)	CHO[c]	SI[d]
25	H	(4-CF_3)$C_6H_4CH_2$	D	0.19	0.06	0.32	97/91	0.11	62/41		29.31	154.26
32	H	(4-CF_3)$C_6H_4CH_2$	F	0.78	0.30	0.39	95/30	0.99	14/0		18.80	24.10
33	H	(4-CF_3)$C_6H_4CH_2$	G	0.40	0.23	0.58	96/45	0.92	62/0		30.03	75.07
34	H	(4-CF_3)$C_6H_4CH_2$	J	0.15	0.05	0.33	89/69	0.056	10/0	1.90	>50	>333
35	H	(4-CF_3)$C_6H_4CH_2$	K	0.28	0.11	0.39	91/66	0.43	8/2	>5	33.81	120.75
36	H	(4-CF_3)$C_6H_4CH_2$	L	0.28	0.06	0.21	92/44	0.59	0/0		36.28	129.57
37	H	(4-CF_3)$C_6H_4CH_2$	M	0.17	0.19	1.12	90/74	0.097	10/0	>5	>50	>294
38	H	(4-CF_3)$C_6H_4CH_2$	N	1.84	0.38	0.21	59/7	3.06	1/0		>50	>27
39	5,6-F	(4-CF_3)$C_6H_4CH_2$	F	0.26	0.13	0.5	94/86	0.21	24/5	2.33	2.04	7.84

40	5,6-F	(4-CF_3)$C_6H_4CH_2$	G	0.25	0.15	0.6	96/60	0.52	73/0		10.04	40.16
41	5,6-F	(4-CF_3)$C_6H_4CH_2$	K	0.19	0.08	0.42	91/62	0.46	0/0	>5	>50	>263
42	5,6-F	(4-CF_3)$C_6H_4CH_2$	L	0.19	0.09	0.47	70/14	0.69	1/0		>50	>263
43	H	H	G	0.20	0.79	3.95	47/0		39/31		33.30	166.5
44	H	H	K	0.30	0.88	2.93	23/0		31/22		>50	>166
45	H	H	L	0.27	0.63	2.33	0/0		0/0		>50	>185
46	H	H	P	0.08	0.25	3.125	56/30		0/0		30.46	>380
47	5,6-F	H	G	0.26	0.83	3.19	31/0		0/0		16.65	64.03
48	5,6-F	H	K	0.25	0.78	3.12	35/0		0/0		>50	>200
49	5,6-F	H	L	0.26	0.53	2.40	16/0		0/0		39.74	152.84
50	5,6-F	H	P	0.15	0.28	1.87	0/0		0/0		34.15	227.66
51	4,6-Cl	H	G	0.22	0.40	1.81	0/0		0/0		25.78	117.18
52	H	(4-CF_3)$C_6H_4CH_2$	Q	5.47			38/20		0/0		47.56	10.45
Chloroquine			0.01	0.42		42.00						
Emetine											0.02	
Methylene blue							93[e]	0.19	90[e]	0.14		

[a]ABS = Asexual Blood Stage, IC_{50}s represent mean from n values of ≥2 independent experiments; [b]RI = resistance index (ratio of IC_{50} [K1]: IC_{50} [NF54]), [c]CHO = Chinese hamster ovarian cell line; [d]SI = selectivity index (ratio of IC_{50}[CHO]: IC_{50}[NF54]); [e]%Inhibition at 1 µM; Dual-point values were determined for one biological repeat (n=1), in technical triplicates. IC_{50} values are means from at least three independent biological repeats (n ≥ 3) performed in technical triplicates. Blank spaces = not tested

The effect of the synthesized compounds on *P. falciparum* gametocyte viability was investigated using the transgenic parasite line, NF54-*Pfs*16-GFP-Luc, in a luciferase reporter assay,[24] allowing for stage-specific determination of gametocytocidal action. Dual point screens of each compound were performed at concentrations of 1 and 5 μM (Table 1) against early-stage (50% stage II/50% stage III) and late-stage gametocytes (40% stage IV/60% stage V). Compounds exhibiting good potency (>70% inhibition at 5 μM and >50% inhibition at 1 μM), were progressed to dose dependent IC_{50} determinations.

From Table 1, the 1-benzylbenzimidazole series showed better potency against early-stage gametocytes than to later stages. Analogues based on the *ortho*-hydroxy aniline Mannich base (R' = C, Table 1) and its derivatives (R' = D, E) displayed good activity (>70% inhibition) against early-stage but not late-stage gametocytes at the 5 μM drug concentration. Generally, the 1-((4-trifluoromethyl)benzyl) and 1-(4-fluorobenzyl) analogues were more potent (>90% inhibition at 5 μM) than their corresponding 1-(4-cyanobenzyl) congeners, which displayed moderate activity. The frontrunner compound 25 maintained >90% inhibition at 1 μM and recorded an IC_{50} value of 0.11 μM towards early-stage gametocytes. Compounds 24, 29, and 30 also showed good IC_{50} values of 1.45 μM, 2.23 μM, and 0.88 μM, respectively. Similarly, the SAR 2 congeners of 25 exhibited <1 μM IC_{50} values, except 38. Moreover, 34 and 37 demonstrated potent activity with IC_{50} values of 0.056 μM and 0.097 μM, comparable to 25 (IC_{50} = 0.11 μM), corroborating the earlier finding in ABS activity (for SAR 2) above that the C5' methyl group on the phenol unit can be replaced by the chloro and fluoro groups with retention of activity.

Compounds with early-stage gametocytocidal activity of IC_{50} <0.5 μM were prioritized for IC_{50} determinations against late-stage gametocytes. In this regard, only 34 (IC_{50} = 1.90 μM) and 39

(IC_{50} = 2.33 µM) showed moderate activities (Table 2). Key compounds (24, 25, 34, 35, 37, 39, and 40) were further screened for their potential transmission blocking activity against male gametes at 2 µM but the compounds showed <50% inhibition of male gamete exflagellation. The poor activity of these compounds towards the transmissible gamete stages correlates with the lack in potency observed against the late-stage gametocytes, confirming their specificity towards early-stage gametocytes.

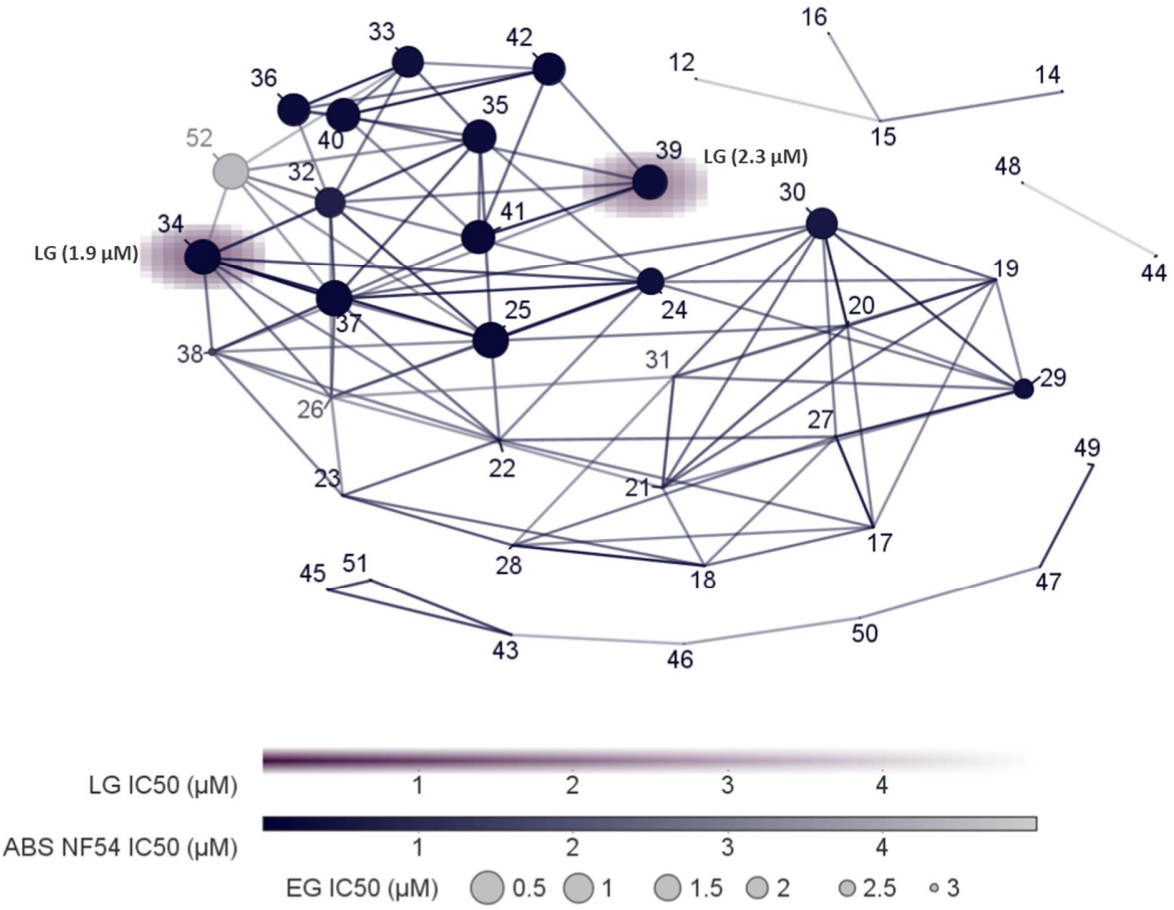

Figure 3: Structure–activity landscape index (SALI) plot of the 1-benzylbenzimidazoles and 1*H*-benzimidazole analogues. Pairwise structural feature (SkelSphere) of asexual blood stages (ABS) and late-stage (LG, IV/V) analysis superimposed with early-stage (EG, I-III) cliff analysis (Osiris DataWarrior) at a similarity threshold of 86%. Activity

inclusions include hit IC_{50} (μM) of asexual blood stages (ABS), early- (EG) and late-stage (LG) gametocytes. Clusters indicate structurally related compounds, with compounds indicated as nodes, and structural connectivity indicated through the edges. Node size reflects IC_{50} values against EG, node color and shadow (clouds) indicate activity ABS LG, respectively.

To summarize, Figure 3 depicts a structure-activity landscape evaluation showing a clear chemically distinct profile between the synthesized 1-benzylbenzimidazole (17 – 42, 52) and 1*H*-benzimidazole (12 – 16 and 43 - 51) analogues with respect to antiplasmodium activity. That is, the 1-benzylbenzimidazoles showing ABS and early-stage gametocyte dual-activities from both SAR 1 and SAR 2 clustered separately from the less active 1*H*-benzimidazoles. Within the 1-benzylbenzimidazole cluster, from SAR 1, compounds containing either the 3-((*N*,*N*-diethylamino)methyl)-2-hydroxy aniline (R' = C, Table 1) or its 5-methyl congener (R' = D, Table 1) Mannich bases derivatized with either 1-((4-trifluoromethyl)benzyl)benzimidazole (as in 24 and 25) or the 1-(4-fluorobenzyl)benzimidazole (as in 29 and 30) groups showed the most potent ABS and early stage gametocyte (EG) activity. Subsequent SAR 2 analogues (32 – 42) based on compound 25 maintained their respective ABS and EG dual-activities with IC_{50}'s < 1 μM, as they clustered closely with 25 (Figure 3). Meanwhile, all other Mannich base side chains (that is, R' = A, B and E; Table 1) and analogues derived from the 1-(4-cyanobenzyl)benzimidazole scaffold constituted a less active cluster. Furthermore, Figure 3 also confirms the strong selectivity of the present benzimidazole compounds towards early-stage compared to late-stage gametocytes, with only two compounds (34 and 39) showing moderate late-stage gametocyte activity (IC_{50}'s between 1-5 μM, Table 2).

Cytotoxicity: The toxicity of the synthesized compounds to mammalian cells was assessed against the Chinese hamster ovarian (CHO) cell line. The compounds were relatively non-cytotoxic, exhibiting acceptable selectivity indices (SI>10), except 39 (Tables 1 and 2). Meanwhile, representative compounds were evaluated for toxicity against the Caucasian hepatocellular carcinoma cells, HepG2 (Supplementary Information file 1, Table S1).

Metabolic stability in liver microsomes and physicochemical properties: Compounds 25, 32, and 33 were assessed for metabolic stability in mouse, rat, and human liver microsomes (MLM, RLM, and HLM, respectively). Compounds with >70% remaining after 30 minutes of incubation with liver microsomes were adjudged to be metabolically stable. The compounds showed species-specific metabolism with respect to rodents and humans (Table 3). The compounds were more stable in HLM than MLM and RLM. Compound 25 was, however, much more rapidly metabolized compared to 32 and 33.

Metabolite identification studies on 25 in MLM revealed that it underwent two main metabolic processes involving oxidation of either the benzimidazole core or the phenol unit, and deethylation of the aminoalkylmethylene moiety (Figure 4A). Analyses of the relative proportions of the metabolites, however, revealed that the *N*-desethyl metabolite of 25 (the equivalent of 32) is rapidly formed and hence a major contributor to the loss of 25 (Figure 4B), which is congruent to the metabolism of amodiaquine to its active metabolite, desethyl amodiaquine.[25] A substantial proportion of the oxidized metabolite (P+16) was formed, which is comparable to the P-12 metabolite, most likely formed after oxidation of the *N*-desethyl metabolite (P-28 [32]). Like desethyl amodiaquine, the antiplasmodium activity of 32 (IC_{50} *Pf*NF54/K1 = 0.78/0.30 µM, Table 2) has useful pharmacological significance. The low relative abundance of the

dideethylation metabolite (P-56), formed either directly from the parent molecule or after further deethylation of P-28, suggests that its formation is not a rapid process (Figure 4B). However, it is noteworthy that this metabolite (P-56 [52, IC_{50} *Pf*NF54 = 5.47 µM], Table 2) was about six- and twenty-four-fold less active than the desethyl (P-28, 32) and diethyl (25) congeners, respectively. Further, in contrast to rapid metabolism of the Mannich base side chain of 25 and 32, the *N*-*t*-butyl moiety of 33 was stable to metabolism, thus only the oxidized metabolite was observed (Figure 4C).

Table 3: *In vitro* microsomal stability and physicochemical properties of selected analogues

Compound	Metabolic stability (% remaining after 0.5 h)			cLogP[a]	Solubility (µM) pH6.5
	MLM	RLM	HLM		
25	<7	<7	36	7.0	<5
32	52	51	98	6.0	35
33	62	41	99	6.7	50
35	73	66	94	6.3	12
36	36	9	81	7.0	<5
39	93	77	99	6.2	16
40	>99	89	90	7.0	<5
41	86	98	>99	6.6	<5
42	94	94	89	7.3	<5
44	97	98	93	3.9	200
48	98	>99	>99	4.2	12

[a]Predicted from ChemDraw Professional, version 19.0

A.

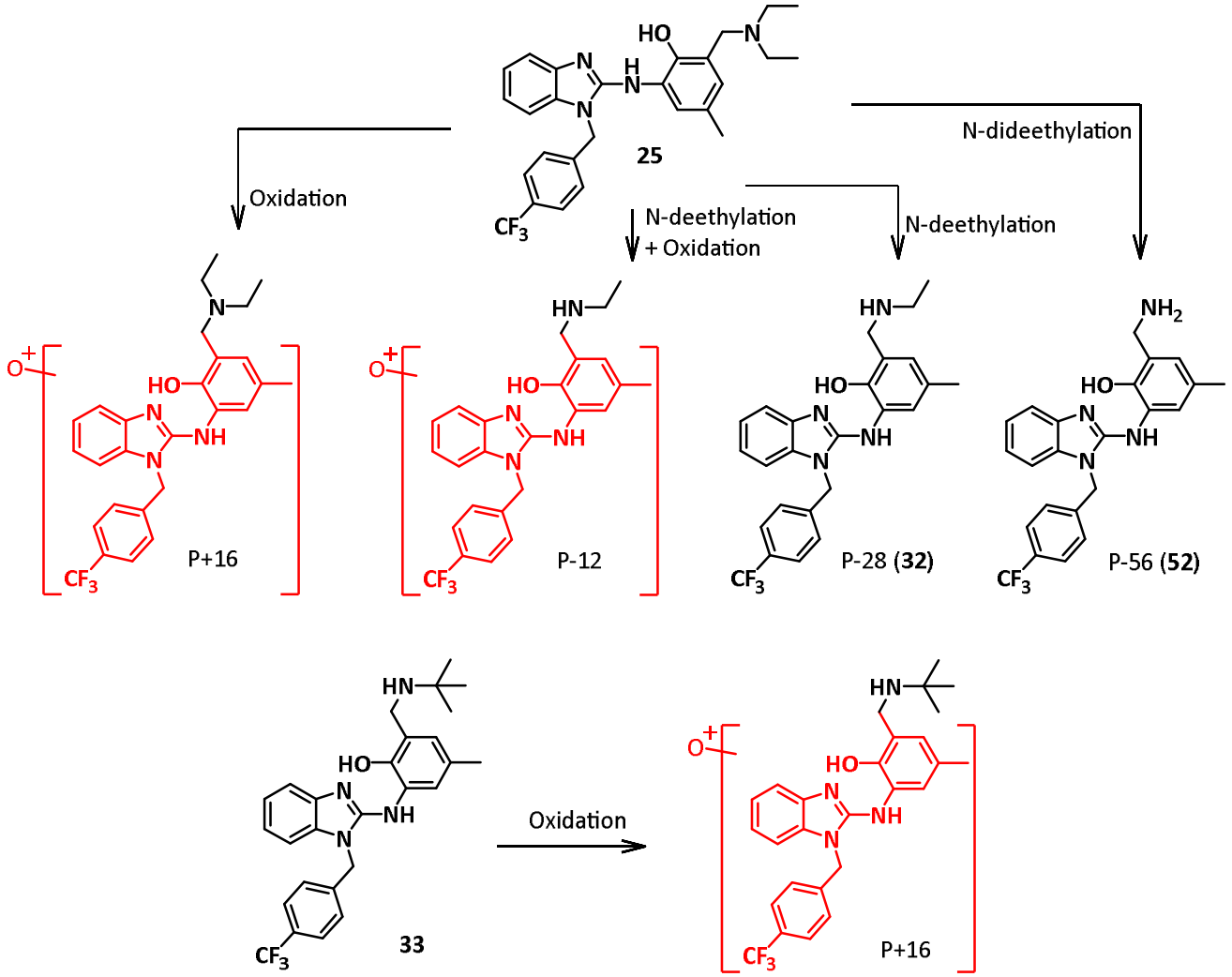
25
Oxidation
N-deethylation
+ Oxidation
N-deethylation
N-dideethylation
P+16
P-12
P-28 (32)
P-56 (52)
33
Oxidation
P+16

B)

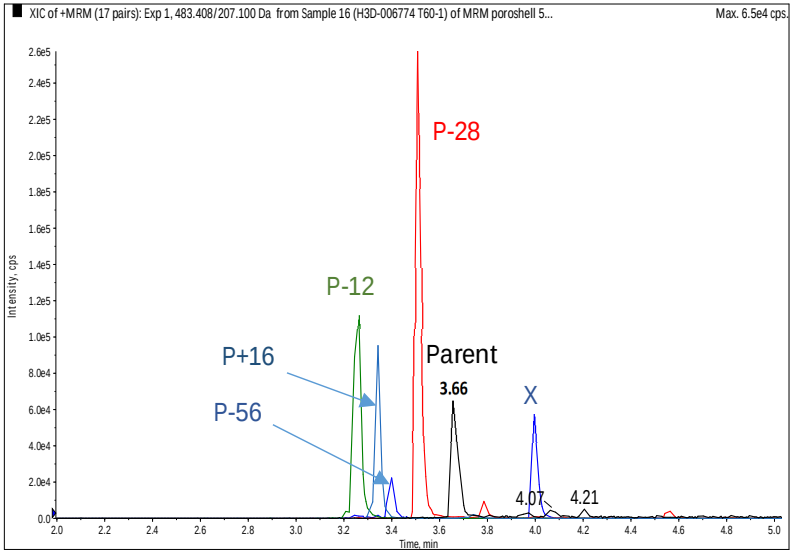

C)

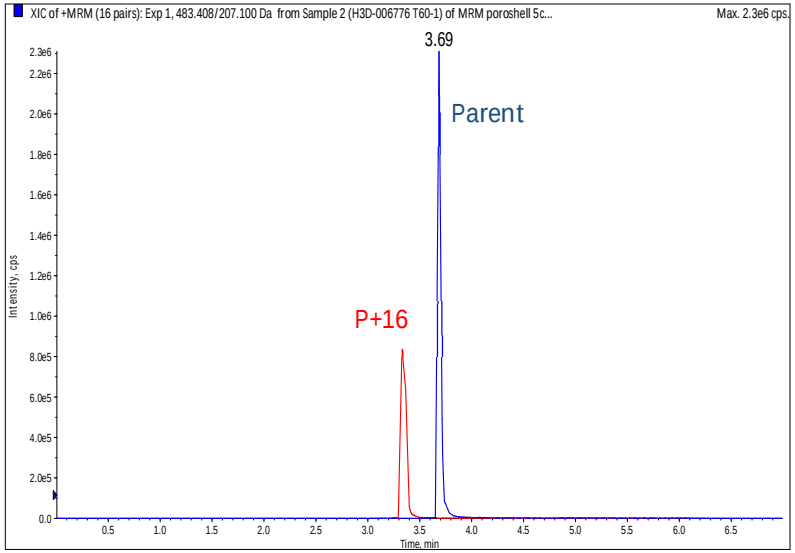

Figure 4: A) Identified metabolites from the metabolism of the parent (P) compounds 25 and 33 in mouse liver microsomes (MLM); B) An XIC plot showing the relative abundances of the identified metabolites from 25; C) An XIC plot showing the relative abundance of 33 and its only metabolite (P+16) in MLM.

From Figure 4, selected compounds were assessed for further metabolic stability studies in MLM, RLM and HLM with the aim to investigate and mitigate the formation of the oxidized metabolite (P+16). The compounds were selected based on the hypothesis that the oxidation arose from hydroxylation of either the benzene unit of the benzimidazole core or the methyl group on the phenol unit. In this regard, all the selected compounds showed improved stability in liver microsomes in all the three species compared to the parent compounds (32 and 33, [Table 3]). That is, fluoro substitution on the benzimidazole core (as in 39 and 40) resulted in higher stability than the replacement of the methyl group on the phenol unit with a chloro group (as in 35 and 36). Further, substitutions at both sites, as in compounds 41 and 42, afforded the most metabolically stable analogues. The results suggest that oxidation on the benzimidazole core is more detrimental to stability in liver microsomes than on the phenol unit. However, from the results of 44 and 48, which lack the benzyl moiety on the benzimidazole core, it is apparent that the presence of the benzyl group makes the benzimidazole core scaffold more susceptible to metabolism *via* oxidation. In this regard, the possibility of the oxidation happening at the benzylic position rather than on the benzimidazole core cannot be overlooked.

Compounds selected for microsomal metabolic stability studies were also profiled for aqueous solubility at a pH of 6.5 (Table 3). As expected, fluorination of the benzimidazole core scaffold and substitution of the 5'-methyl group with the chloro group on the phenol moiety led to poor aqueous solubility. Compound 44, which lacks the benzyl and fluoro groups on the benzimidazole core, was highly soluble (200 µM) compared to 41 (<5 µM) and 48 (12 µM), thus highlighting the expected negative contributions of these groups to solubility.

In vivo efficacy studies: Six compounds with good antiplasmodium activity and MLM stability were evaluated for *in vivo* efficacy in a *P. berghei*-infected NMRI mouse model (Table 4). Compounds were dosed orally at 4×50 mg/kg. Parasitemia reduction was expressed as a percentage relative to the control. The only exception was compound 41, which achieved an encouraging parasitemia reduction of 98%. Interestingly, no apparent correlation could be deduced between the observed *in vivo* efficacy results and the *in vitro* ABS activity, hepatic microsomal stability, and solubility of the test compounds (Table 4).

Table 4: *In vivo* antimalarial efficacy after 1 oral dose of 50mg/kg on four consecutive days in *P. berghei*-infected mice

Compound	*Pf*NF54, IC_{50} µM	MLM, (%)	Solubility, pH6.5 (µM)	% Activity
33	0.40	62	50	<40
35	0.28	73	12	<40
41	0.19	85	<5	98
42	0.19	94	<5	<40
44	0.30	97	200	<40
48	0.25	98	12	<40
Chloroquine[a]				99.9
[a]oral dose, 4×30 mg/kg				

Pharmacokinetics studies: To ascertain the possible underlying reasons for the lack of *in vivo* efficacy, such as drug absorption, permeation and exposure-related shortfalls, pharmacokinetics studies were carried out in healthy Balb/c mice using two representative compounds, 41 and 48 (Table 5). A higher oral exposure was measured for 41 as compared to 48 (Figure 5). Given that the antiplasmodium activity is comparable between the two compounds, this difference in exposure could explain the lower efficacy of 48. The clearance of 41 is also markedly lower than

the clearance of 48 with the latter clearance being higher than hepatic blood flow. This suggests extrahepatic routes of clearance or the involvement of active transporters in the clearance of 48.

Table 5: Intravenous (i.v) and oral (p.o) mouse pharmacokinetics parameters for 41 and 48

	41		48	
Route	i.v	p.o	i.v	p.o
Nominal Dose (mg/kg)	3	10	3	10
C_{max} (μM)		0.4		0.026
T_{max} (h)		2.8		0.7
$t_{1/2}$ terminal (h)	6.3	8.3	ND	ND
Clearance CL_b (mL/min/kg)	12.6		151	
V_d (L/kg)	6.9		96	
V_{ss} (L/kg)	5.8		58	
AUC_{0-t} (min·μmol/L)	443	321	65	11
F (%)		24		5
Blank spaces = not determined				

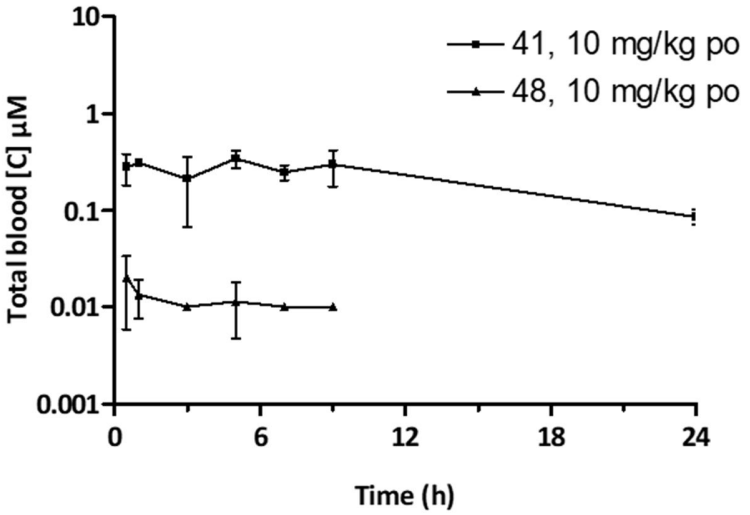

Figure 5: Pharmacokinetics profile of 41 and 48 following oral administration. Each data point represents the mean from 3 mice with error bars indicating the standard deviation.

Permeability studies: To further investigate the contribution of physicochemical parameters to the pharmacokinetics profiles of the compounds the permeability of model compounds 35 and

44 was investigated using the parallel artificial membrane assay (PAMPA, Table 6). It was not possible to get reproducible data for the same compounds for which pharmacokinetic studies had been performed due to their poor solubility under the assay conditions.

Table 6: *In vitro* permeability studies for 35 and 44

Compound	Permeability ($LogP_{app}$)
35	-5.1
44	-6.2

As expected from the cLogP data (Table 3), 35 was more permeable than 44, with the two compounds falling into the moderate and low permeability classes, respectively. Improved permeability is associated with better passive permeability through the body and with a reduced contribution by active transport processes to both absorption and clearance.[26,27] If the same trends hold across the series, 48 would be expected to be less permeable than 41 and thus more prone to active transport contributions to its clearance, thus explaining lower exposure.

Mechanistic studies: Antimalarial benzimidazole derivatives have recently been shown to inhibit hemozoin formation.[16,28,29] Thus, inhibition of hemozoin formation as a potential mode of action of the synthesized analogues in ABS parasites was first evaluated *in vitro* by investigating their ability to inhibit the formation of β-hematin, the synthetic equivalent of hemozoin, in a cell-free assay. Most compounds passed a discriminatory cut-off of β-hematin inhibition activity (βHIA) at IC_{50} <100 µM and were therefore classified as good inhibitors of ß-hematin formation (Supplementary Information Table S1).

To validate the above, a cellular heme fractionation assay was further carried out to determine if these compounds are true inhibitors of hemozoin formation. In this regard, four compounds, 35, 41, 44 and 48, having βHIA IC_{50} values of 33.31, 18.14, 12.71 and 7.15 μM, respectively, compared to amodiaquine (IC_{50} βHIA = 13.16 μM), were chosen for investigation in this assay, which measures the free heme and hemozoin levels when synchronized ring-stage parasites are treated with increasing concentrations of the compounds. For true inhibitors of hemozoin formation, a dose-dependent increase in free heme is observed with a concomitant decrease in hemozoin.[30] From Figure 6, compounds 44 and 48 were identified as bona fide hemozoin inhibitors. However, 35 and 41, despite their ability to inhibit β-hematin in the cell-free assay, showed no significant concentration-dependent effect on the heme and hemozoin levels in the cellular fractionation assay (Figure 6).

Taken together, the results suggest hemozoin inhibition as one of the mechanisms by which 44 and 48 act. However, inhibition of hemozoin formation is not the sole mode of action of the current compounds since 35 and 41 do not directly act on this pathway.

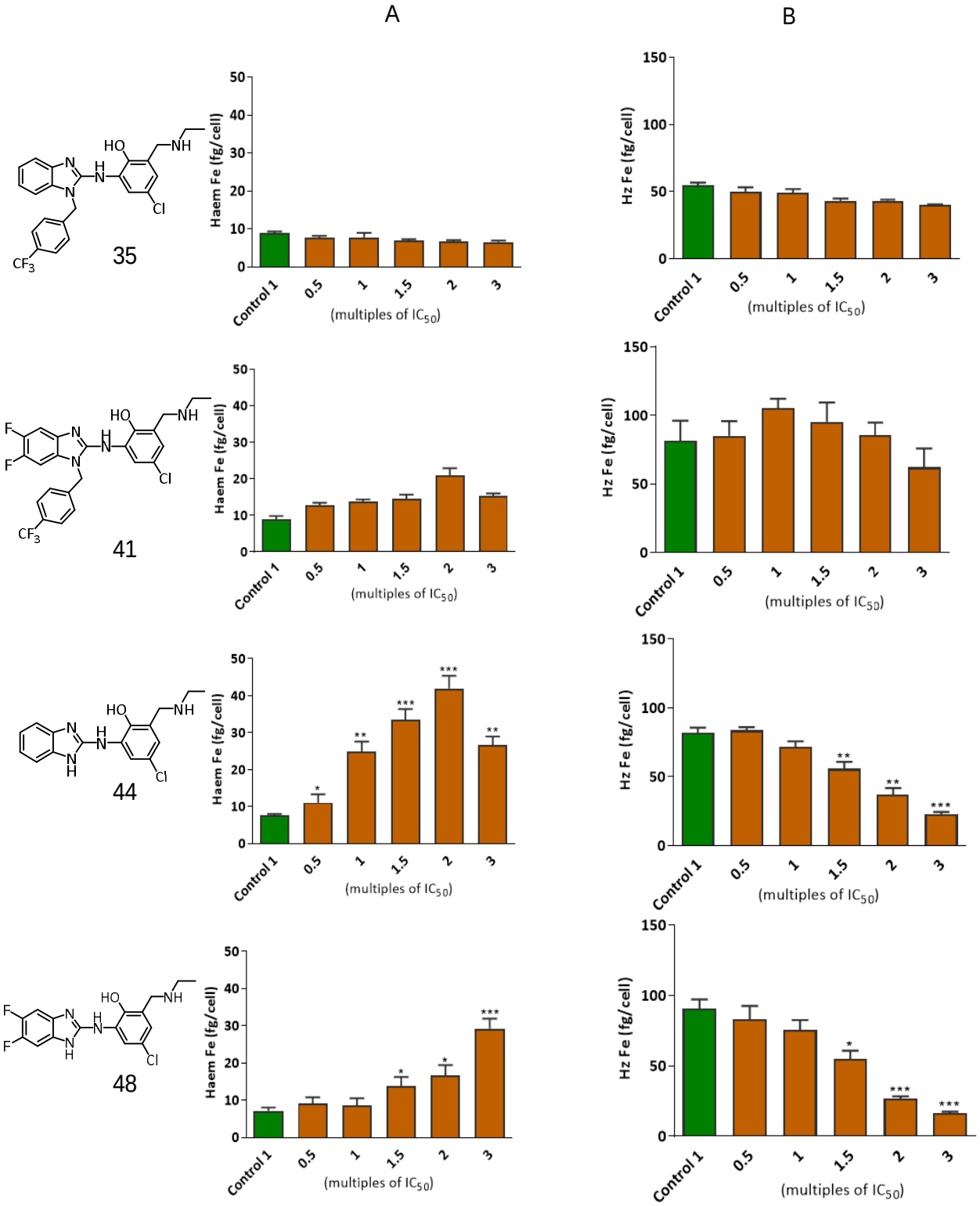

Figure 6: Heme species in synchronized control and drug treated *Pf*NF54 parasites. Plots A and B represent free heme and hemozoin, respectively, represented in terms of iron (Fe) measured in fg/cell. Asterisks indicate statistical

significance relative to the control, where $p < 0.05$ (*), $p < 0.01$ (**), and $p < 0.001$ (***) [Supplementary information file 1, Figures S2 – S5].

In further mechanistic studies, compounds 41 and 44 were investigated for the potential to inhibit microtubule formation in *P. falciparum* ABS and early-stage gametocytes, with colchicine as positive control (Figure 7). This was prompted by knowledge of anthelminthic benzimidazole drugs, which bind to the colchicine site and inhibit microtubule assembly between α and β-tubulin, through interacting with the β-tubulin subunit.[31,32] Microtubules are present during all ABS, and in gametocytes, microtubules play key roles in the morphological changes associated with parasite development from stage I-IV, but disassembles in stage V.[33] For this reason, these cytoskeletal proteins have long been known as a potential drug target for malaria treatment although not extensively explored.[32–35] This further prompted us to investigate inhibition of microtubule formation as a potential contributing mechanism.

Live cell confocal microscopy of treated ABS parasites and early-stage gametocytes stained with Tubulin Tracker showed a marked decrease in tubulin density in ABS parasite stages (Figure 7A and B, Supplementary Information file 1, Figures S6 and S7), similar to that observed for colchicine, indicating that the compounds are able to inhibit tubulin polymerization. Interestingly, colchicine inhibited microtubule polymerization from stage I gametocyte development, with 41 and 44 treatment only showing little or no apparent decrease in Tubulin Tracker® signal intensity in stage I gametocytes compared to untreated parasites. However, all three compounds decreased tubulin formation from stage II and III gametocytes, amongst which, 41 showed the most significant decrease in Tubulin Tracker® intensity, with signal only limited to

the periphery of the parasite (Figure 7B). Between 41 and 44, these results support the high *in vitro* early-stage gametocytocidal activity (Tables 1 and 2) of the 1-benzylbenzimidazole series.

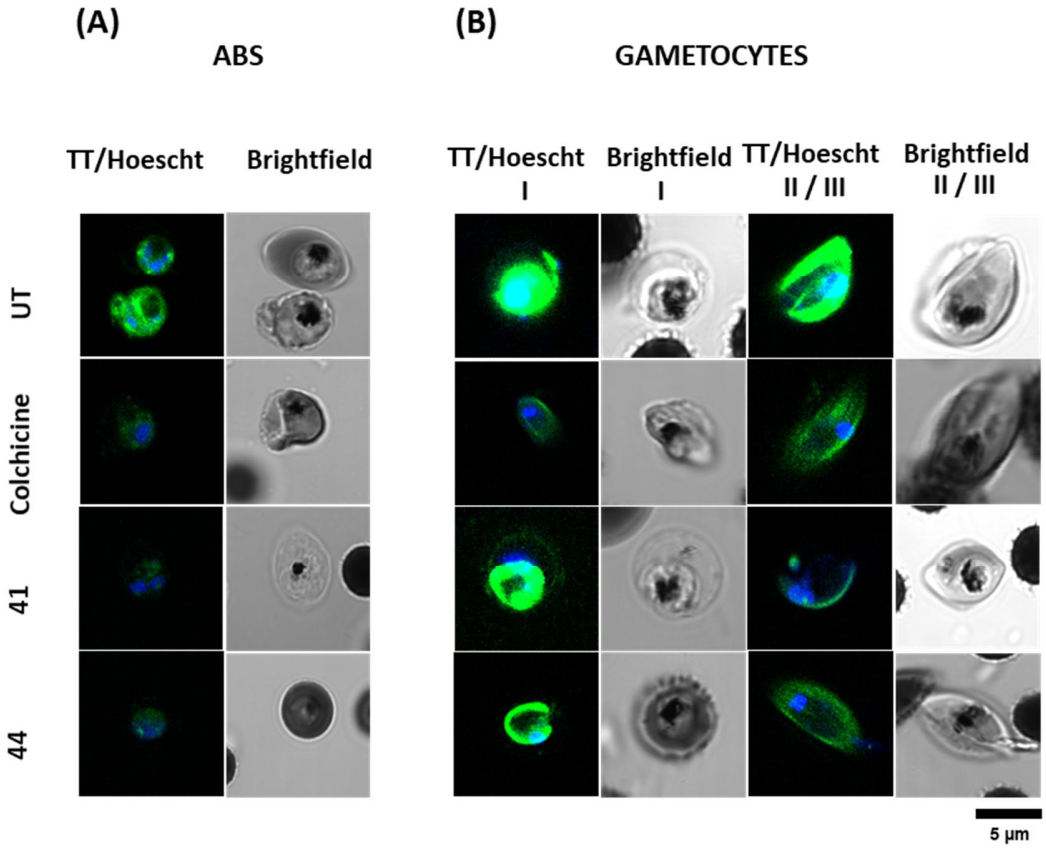

Figure 7: Inhibition of microtubule formation in asexual trophozoites (A) and stage I-III gametocytes (B). Live cell confocal imaging of asexual trophozoites and early-stage gametocytes (20% stage I/ 60% stage II/20% stage III) labelled with Tubulin Tracker® (TT, green) and Hoescht 3324 nuclear stain (blue). Brightfield images are shown on right side of each image. UT = Untreated. Scale represents 5 µm.

Although potent microtubule destabilizers, colchicine (IC_{50} = 10 µM) and colchicine-site binders, such as albendazole (IC_{50} = 30 µM), mebendazole (IC_{50} = 200 µM), and nocodazole (IC_{50} = 17 µM), are less active against *P. falciparum* ABS and show low therapeutic indices (0.001 - 0.01) relative to mammalian cells.[34] The poor antiplasmodium activity of these benzimidazole drugs is due to poor binding to β-tubulin (the presence of Met rather than Val or Ile in *P. falciparum* β-tubulin

position 316).[32] Further, *P. falciparum* gametocytes are insensitive to colchicine,[36] although in *P. yoelii nigeriensis* gametocytes, colchicine was shown to inhibit the polymerization of cytoplasmic-axonemal- and intranuclear mitotic-microtubules, but male and female gametocytes remained unchanged at inhibitory concentrations of the drug.[37] On the contrary, however, coupled with microtubule activity (Figure 7), the benzimidazoles presented here show potent ABS activity (Tables 1 and 2) and the 1-benzylbenzimidazole series exhibit activity as low as IC_{50} = 56 nM (compound 34) against stage II/III gametocytes, with good selectivity margins (SI >10). Furthermore, the lack of microtubule inhibition in stage I gametocytes by the present benzimidazoles contrary to colchicine (Figure 7B), and yet a significant microtubule activity in stage II/III gametocytes, clearly suggests that the former affect gametocyte microtubule structures in a different manner to colchicine, halting polymerization and/or decreasing tubulin population, possibly by inducing microtubule catastrophe, from stage I gametocytogenesis onwards, which could arrest further development. In effect, it would be worth investigating in much more detail the inhibitory effects of the potent benzimidazoles presented here against ABS and early-stage gametocytes microtubules, bearing in mind that the functions of these cytoskeletal proteins are not only limited to their role in cell division. If the current benzimidazoles are bona fide inhibitors of microtubules, then the lack of late stage gametocytocidal activity could be related to disassembled microtubules, especially in stage V gametocytes.[33]

CONCLUSION

Novel benzimidazole analogues incorporating phenolic Mannich base side chains were synthesized and evaluated as potential antimalarial agents. Most of the analogues showed

antiplasmodium activity against the NF54 and K1 strains of *P. falciparum* with IC_{50} values <1 μM, as well as acceptable selectivity margins with respect to cytotoxicity. The 1-benzylated benzimidazole analogues exhibited early-stage gametocytocidal activity with IC_{50} values <1 μM. One analogue (41) showed 98% activity in *P. berghei*-infected mice after 1 oral dose of 50 mg/kg on four consecutive days. The synthesized analogues showed inhibitory activity against hemozoin formation and microtubule polymerization (in trophozoites and early-stage II/III gametocytes). The strategy and plans for a future lead optimization campaign to improve potency, maintain favorable ADME-PK properties, limit cytotoxicity and improve efficacy will include SAR expansion around the benzimidazole scaffold, benzylic group, and the Mannich base side chain.

EXPERIMENTAL SECTION

The starting reagents, 2-chloro benzimidazole, 1-(4-fluorobenzyl)-2-chlorobenzimidazole and the amino phenols, were purchased from commercial vendors. Unless otherwise stated, all solvents used were anhydrous. Reactions were monitored using aluminum silica pre-coated thin layer chromatography (TLC) plates (Silica gel 60 F_{254} (Merck KGaA, Darmstadt, Germany)). TLC spots were visualized under ultraviolent light (UV) at 254 nm. ^{1}H-NMR and ^{13}C-NMR spectra were acquired on either a Bruker AV 400 (^{1}H 400.0, ^{13}C 100.6 MHz) or Bruker Ascend™ 600 (^{1}H 600.0, ^{13}C 151 MHz) spectrometers. An Agilent LC-MS instrument comprising an Agilent 1260® Infinity Binary Pump, Agilent 1260® Infinity Diode Array Detector, Agilent 1290® Infinity Column Compartment, Agilent 1260® Infinity Autosampler, Agilent 6120® Quadrupole MS, and Peak Scientific® Genius 1050 Nitrogen Generator, and fitted with an X-bridge® (C18, 2.5 μm, 3.0 mm (ID) x 50 mm length) column maintained at either 35 or 40 °C was used to monitor the progress

of reactions including percent purity determinations. Target compounds were confirmed to have >95% purity.

General synthetic procedure I (2 and 3): A mixture of 2-chloro-1*H*-benzimidazole (1 eq.) and the corresponding benzyl bromide (1.1 eq.) in acetonitrile were refluxed at 75 ^{o}C in the presence of K_2CO_3 (1.1 eq.) as base. Upon completion (TLC, 2 h), the reaction mixture was allowed to cool, diluted with DCM, filtered and the filtrate removed *in vacuo* to obtain a white amorphous solid residue. The residue was triturated with diethyl ether to remove unreacted benzyl bromide. The benzylated benzimidazole intermediates (2 and 3) were used for the next reaction without any further purification.

General synthetic procedure II (5 and 6): A mixture of urea and the corresponding 1,2-benzenediamine in THF was irradiated at 130 ^{o}C under microwave conditions for 30 mins. The precipitate formed was triturated with diethyl ether and the amorphous solid (5 or 6) was used in the subsequent reaction without any further purification.

General synthetic procedure III (7): Compound 7 was synthesized from 5 according to the general synthetic procedure I.

General synthetic procedure IV (11a-m): A mixture of the corresponding hydroxyaniline (8a-i, 1.0 eq.) and acetic anhydride (1.5 eq.) in THF was heated at 60 ^{o}C for 1 h. After completion of reaction (TLC and LCMS), solvent was removed under reduced pressure and residue was triturated with diethyl ether to obtained *N*-(hydroxyphenyl) acetamides (9a-i). The acetamides (1 eq.) were dissolved in EtOH (10 mL) and heated (80 ^{o}C) with *N*,*N*-diethylamine, *N*-ethylamine or *N*-*tert*-butylmine (1.5 eq) and formaldehyde (1.5 eq.) until completion (TLC, 2 h). The solvent

was removed *in vacuo*. The residue was dissolved in DCM (20 mL) and acidified with 1M HCl (15 mL). The aqueous layer was separated through a separating funnel and basified with a saturated solution of NaOH to a pH of 8-10. This was followed by extraction of the target compound with DCM (2×20 mL). The combined organic phase was dried over anhydrous Na_2SO_4. After filtration, the solvent was removed under reduced pressure to obtain compounds 10a-m. Compounds (2 mmol) were refluxed in 6N HCl (2 mL) at 100 °C for 2 h (TLC). Solvent was removed under reduced pressure. The residue was dissolved in EtOH (2×15 mL) and solvent was removed *in vacuo* to obtain the corresponding *N*-deacetylated Mannich base products 11a-m (as HCl salt).

General synthetic procedure V (12-51): A mixture of the corresponding benzimidazole (1-7) (1.0 eq.) in *n*-BuOH and the respective phenolic Mannich base (11a-m) (1.1 eq.) in *n*-BuOH was heated at 100 °C in the presence of excess KH_2PO_4 as base. Upon completion (TLC, 8-16 h), the reaction mixture was allowed to cool, diluted with water and the solvent was removed under reduced pressure. The residue was dissolved in a mixture of DCM: MeOH 1:1 *v/v* and completely dried in the Genevac to remove all traces of *n*-BuOH. The target compounds (12-51) were obtained after flash column chromatography using mixtures of DCM and MeOH as mobile phase.

2-(3-((*N*,*N*-diethylamino)methyl)-4-hydroxyanilino)-1*H*-benzo[*d*]imidazole (12): Brown viscous oil (82 mg, 41% yield); ^{1}H NMR (400 MHz, DMSO-d_6) δ 7.69 (d, *J* = 2.7 Hz, 1H), 7.46 (dd, *J* = 3.2, 5.9 Hz, 2H), 7.35 (dd, *J* = 2.7, 8.7 Hz, 1H), 7.21 (dd, *J* = 3.2, 5.9 Hz, 2H), 7.13 (d, *J* = 8.6 Hz, 1H), 4.25 (s, 2H), 3.14 (q, *J* = 7.1 Hz, 4H), 1.31 (t, *J* = 7.1 Hz, 6H); ^{13}C NMR (101 MHz, DMSO-d_6) δ 154.5, 148.3, 130.8 (2C), 127.9, 126.8, 125.6, 122.7 (2C), 117.1, 116.8, 111.8 (2C), 49.5, 46.0 (2C) and 8.3 (2C); LC-MS (ESI): *m/z* 311.1 $[M+H]^+$; purity (LC-MS): 98%, t_R = 0.38 min.

2-(4-((*N*,*N*-diethylamino)methyl)-3-hydroxyanilino)-1*H*-benzo[*d*]imidazole (13): Brown viscous oil (71 mg, 35% yield); ^{1}H NMR (600 MHz, MeOH-d_4) δ 7.59 (br s, 2H), 7.46 (d, *J* = 8.1 Hz, 1H), 7.16 (dd, *J* = 3.1, 5.9 Hz, 2H), 6.91 (d, *J* = 2.1 Hz, 1H), 6.88 (dd, *J* = 2.2, 8.1 Hz, 1H), 4.31 (s, 2H), 3.26 (q, *J* = 7.2 Hz, 4H), 1.40 (t, *J* = 7.2 Hz, 6H); ^{13}C NMR (151 MHz, MeOH-d_4) δ 159.2, 152.5, 142.2, 135.1 (2C), 123.4 (2C), 113.9 (2C), 112.3 (2C), 108.1 (2C), 52.5, 48.7 (2C) and 9.3 (2C); LC-MS (ESI): *m/z* 311.1 $[M+H]^+$; purity (LC-MS): 98%, t_R = 0.33 min.

2-(3-((*N*,*N*-diethylamino)methyl)-2-hydroxyanilino)-1*H*-benzo[*d*]imidazole (14): Brown semi-solid (81 mg, 40% yield); ^{1}H NMR (600 MHz, MeOH-d_4) δ 7.86 (dd, *J* = 1.5, 7.9 Hz, 1H), 7.28 (dd, *J* = 3.3, 6.6 Hz, 2H), 7.03 (dd, *J* = 3.3, 6.6 Hz, 2H), 6.77 (t, *J* = 7.7 Hz, 1H), 6.71 (dd, *J* = 1.5, 7.7 Hz, 1H), 3.84 (s, 2H), 2.68 (q, *J* = 7.1 Hz, 4H), 1.13 (t, *J* = 7.1 Hz, 6H); ^{13}C NMR (151 MHz, MeOH-d_4) δ 153.0, 149.3, 129.2 (2C), 123.1 (2C), 122.8, 122.5 , 121.8 (2C), 119.5 (2C), 118.7, 57.7, 47.5 (2C) and 11.5 (2C); LC-MS (ESI): *m/z* 311.1 $[M+H]^+$; purity (LC-MS): 98% , $_R$ = 0.36 min.

2-(3-((*N*,*N*-diethylamino)methyl)-2-hydroxy-5-methylanilino)-1*H*-benzo[*d*]imidazole (15): Yellow semi-solid (110 mg, 52% yield); ^{1}H NMR (600 MHz, MeOH-d_4) δ 7.69 (d, *J* = 1.9 Hz, 1H), 7.29 (dd, *J* = 3.1, 5.8 Hz, 2H), 7.03 (dd, *J* = 3.1, 5.8 Hz, 2H), 6.52 (d, *J* = 1.9 Hz, 1H), 3.77 (s, 2H), 2.65 (q, *J* = 7.1 Hz, 4H), 2.27 (s, 3H), 1.12 (t, *J* = 7.1 Hz, 6H); ^{13}C NMR (151 MHz, MeOH-d_4) δ 153.0, 146.6, 129.1 (2C), 128.8, 123.6 (2C), 122.6, 121.8 (3C), 119.2 (2C), 57.7, 47.5 (2C), 21.0 and11.6 (2C); LC-MS (ESI): *m/z* 325.2 $[M+H]^+$; purity (LC-MS): 98%, t_R = 0.60 min.

2-(3-((*N*,*N*-diethylamino)methyl)-2-hydroxy-6-methylanilino)-1*H*-benzo[*d*]imidazole (16): Brown viscous oil (106 mg, 50% yield); ^{1}H NMR (600 MHz, MeOH-d_4) δ 7.18 (dd, *J* = 3.1, 5.8 Hz, 2H), 6.96 (dd, *J* = 3.1, 5.8 Hz, 2H), 6.90 (d, *J* = 7.7 Hz, 1H), 6.71 (d, *J* = 7.7 Hz, 1H), 3.84 (s, 2H), 2.69

(q, *J* = 7.1 Hz, 4H), 2.24 (s, 3H), 1.11 (t, *J* = 7.1 Hz, 6H); ^{13}C NMR (151 MHz, MeOH-d_4) δ 155.7, 155.6, 138.5, 137.2, 127.8 (2C), 126.1, 121.6 (2C), 121.5, 121.4 (2C), 113.0, 57.2, 47.4 (2C), 18.2 and 11.3 (2C); LC-MS (ESI): *m/z* 325.2 $[M+H]^+$; purity (LC-MS): 98%, t_R = 0.34 min.

1-(4-cyanobenzyl)-2-(3-((*N*,*N*-diethylamino)methyl)-4-hydroxyanilino)benzo[*d*]imidazole (17): Pink semi-solid (150 mg, 94% yield); ^{1}H NMR (600 MHz, MeOH-d_4) δ 7.70 (d, *J* = 8.1 Hz, 2H), 7.63 (d, *J* = 2.6 Hz, 1H), 7.42-7.39 (m, 1H), 7.39-7.35 (m, 3H), 7.20-7.16 (m, 2H), 7.11 (td, *J* = 7.6, 1.0 Hz, 1H), 6.97 (d, *J* = 8.6 Hz, 1H), 5.60 (s, 2H), 4.32 (s, 2H), 2.66 (q, *J* = 7.2 Hz, 4H), 1.39 (t, *J* = 7.2 Hz, 6H); ^{13}C NMR (151 MHz, MeOH-d_4) δ 155.0, 152.5, 142.8, 138.9, 134.2, 133.8 (2C), 132.2, 128.6 (2C), 127.6, 127.0, 123.9, 122.9, 119.4, 118.2, 117.4, 115.9, 112.7, 110.1, 52.5, 48.5 (2C), 46.4 and 9.1 (2C); LC-MS (ESI): *m/z* 426.2 $[M+H]^+$; purity (LC-MS): 98%, t_R = 2.38 min.

1-(4-cyanobenzyl)-2-(4-((*N*,*N*-diethylamino)methyl)-3-hydroxyanilino)benzo[*d*]imidazole (18): Brown semi-solid (87 mg, 55% yield); ^{1}H NMR (600 MHz, MeOH-d_4) δ 7.63 (d, *J* = 8.2 Hz, 2H), 7.43-7.39 (m, 1H), 7.26 (d, *J* = 7.8 Hz, 2H), 7.14-7.07 (m, 2H), 7.05-7.01 (m, 1H), 6.94-6.84 (m, 3H,, 5.49 (s, 2H), 3.73 (s, 2H), 2.63 (q, *J* = 7.1 Hz, 4H), 1.10 (t, *J* = 7.1 Hz, 6H); ^{13}C NMR (151 MHz, MeOH-d_4) δ 160.0, 152.4, 143.7, 142.3, 134.9, 133.7 (2C), 131.6, 130.1, 128.5 (2C), 123.1, 122.0, 119.4, 117.9, 117.5, 112.4, 111.3, 109.6, 108.1, 57.1, 47.3 (2C), 46.3 and 11.6 (2C); LC-MS (ESI): *m/z* 426.2 $[M+H]^+$; purity (LC-MS): 98%, t_R = 2.41 min.

1-(4-cyanobenzyl)-2-(3-((*N*,*N*-diethylamino)methyl)-2-hydroxyanilino)benzo[*d*]imidazole (19): Brown semi-solid (119 mg, 75% yield); ^{1}H NMR (400 MHz, MeOH-d_4) δ 7.74 (dd, *J* = 2.9, 6.5 Hz, 1H), 7.65 (d, *J* = 8.3 Hz, 2H), 7.44-7.40 (m, 1H), 7.36 (d, *J* = 8.3 Hz, 2H), 7.19-7.15 (m, 1H), 7.11 (td, *J* = 7.7, 1.3 Hz, 1H), 7.05 (td, *J* = 7.7, 1.3 Hz, 1H), 6.76-6.69 (m, 2H), 5.47 (s, 2H), 3.82 (s, 2H), 2.67

(q, *J* = 7.2 Hz, 4H), 1.10 (t, *J* = 7.1 Hz, 6H); ^{13}C NMR (101 MHz, MeOH-d_4) δ 152.4, 150.5, 143.3, 142.6, 135.0, 133.8 (2C), 129.3, 128.9 (2C), 123.9, 123.0, 122.6, 122.0, 120.2, 119.4, 119.2, 117.5, 112.7, 109.3, 57.6, 47.4 (2C), 46.4 and 11.3 (2C); LC-MS (ESI): *m/z* 426.2 $[M+H]^+$; purity (LC-MS): 98%, t_R = 2.46 min.

1-(4-cyanobenzyl)-2-(3-((*N*,*N*-diethylamino)methyl)-2-hydroxy-5-methylanilino)benzo[*d*]imidazole (20): Yellow semi-solid (145 mg, 88% yield); ^{1}H NMR (400 MHz, MeOH-d_4) δ 7.64 (d, *J* = 8.0 Hz, 2H), 7.55 (d, *J* = 1.9, Hz, 1H), 7.45-7.40 (m, 1H), 7.35 (d, *J* = 7.8 Hz, 2H), 7.19-7.14 (m, 1H), 7.11 (td, *J* = 7.6, 1.3 Hz, 1H),7.05 (td, *J* = 8.1, 1.3 Hz, 1H), 6.54 (d, *J* = 1.9, Hz, 1H), 5.46 (s, 2H), 3.76 (s, 2H), 2.67 (q, *J* = 7.4 Hz, 4H), 2.23 (s, 3H), 1.09 (t, *J* = 7.1 Hz, 6H); ^{13}C NMR (101 MHz, MeOH-d_4) δ 152.4, 147.7, 143.3, 142.6, 135.0, 133.8 (2C), 128.9, 128.8 (2C), 128.7, 124.4, 123.0, 122.5, 122.0, 120.8, 119.4, 117.4, 112.7, 109.3, 57.5, 47.5 (2C), 46.4, 21.0 and 11.4 (2C); LC-MS (ESI): *m/z* 440.2 $[M+H]^+$; purity (LC-MS): 98%, t_R = 2.54 min.

1-(4-cyanobenzyl)-2-(3-((*N*,*N*-diethylamino)methyl)-2-hydroxy-6-methylanilino)benzo[*d*]imidazole (21): Brown semi-solid (98 mg, 60% yield); ^{1}H NMR (600 MHz, MeOH-d_4) δ 7.67 (d, *J* = 8.1 Hz, 2H), 7.42 (d, *J* = 8.1 Hz, 2H), 7.26-7.23 (m, 1H), 7.07-7.03 (m, 2H), 6.97 (td, *J* = 7.5, 1.1 Hz, 1H), 6.85 (d, *J* = 7.7 Hz, 1H), 6.67 (d, *J* = 7.7 Hz, 1H), 5.49 (s, 2H), 3.80 (s, 2H), 2.66 (q, *J* = 7.1 Hz, 4H), 2.11 (s, 3H), 1.08 (t, *J* = 7.1 Hz, 6H); ^{13}C NMR (151 MHz, MeOH-d_4) δ 155.3, 154.6, 143.8, 142.5, 137.2, 135.4, 133.6 (2C), 128.9 (2C), 127.5, 126.8, 122.7, 121.5, 121.3, 121.2, 119.5, 116.5, 112.4, 109.0, 57.3, 47.3 (2C), 46.2, 18.3 and 11.4 (2C); LC-MS (ESI): *m/z* 440.2 $[M+H]^+$; purity (LC-MS): 98%, t_R = 2.45 min.

1-((4-trifluoromethyl)benzyl)-2-(3-((*N*,*N*-diethylamino)methyl)-4-hydroxyanilino)benzo[*d*]imidazole (22): Pink semi-solid (127 mg, 84% yield); ^{1}H NMR (600 MHz, MeOH-d_4) δ 7.67 (d, *J* = 8.2 Hz, 2H), 7.63 (d, *J* = 2.6 Hz, 1H), 7.46-7.42 (m, 3H), 7.40 (dd, *J* = 2.7, 8.7 Hz, 1H), 7.28-7.25 (m, 1H), 7.23 (td, *J* = 7.6, 1.2 Hz, 1H), 7.18 (td, *J* = 7.6, 1.1 Hz, 1H), 7.02 (d, *J* = 8.6 Hz, 1H), 5.63 (s, 2H), 4.33 (s, 2H), 3.26 (q, *J* = 7.3 Hz, 4H), 1.39 (t, *J* = 7.3 Hz, 6H); ^{13}C NMR (151 MHz, MeOH-d_4) δ 155.9, 152.0, 141.1, 136.3, 133.6, 131.2, 131.0, 128.4 (2C), 126.9 (2C), 125.5, 126.4, 124.6, 124.5, 123.7, 118.6, 117.6, 115.2, 110.6, 52.4, 48.6 (2C), 46.6 and 9.1 (2C); LC-MS (ESI): *m/z* 469.2 $[M+H]^+$; purity (LC-MS): 98%, t_R = 2.59 min.

1-((4-trifluoromethyl)benzyl)-2-(4-((*N*,*N*-diethylamino)methyl)-3-hydroxyanilino)benzo[*d*]imidazole (23): Brown semi-solid (75 mg, 50% yield); ^{1}H NMR (600 MHz, MeOH-d_4) δ 7.59 (d, *J* = 8.1 Hz, 2H), 7.45-7.42 (m, 1H), 7.29 (d, *J* = 8.3 Hz, 2H), 7.17-7.09 (m, 4H), 7.07 (td, *J* = 7.7, 1.1 Hz, 1H), 6.93 (dd, *J* = 2.2, 8.2 Hz, 1H), 5.53 (s, 2H), 4.04 (s, 2H), 2.97 (q, *J* = 7.2 Hz, 4H), 1.25 (t, *J* = 7.2 Hz, 6H); ^{13}C NMR (151 MHz, MeOH-d_4) δ 159.1, 151.9, 144.3, 142.4, 134.9, 132.3, 131.7, 130.9, 128.2, 128.1 (2C), 126.7 (2C), 125.5, 123.2, 122.3, 117.6, 111.4, 109.9, 107.1, 54.5, 48.0 (2C), 46.3 and 10.1 (2C); LC-MS (ESI): *m/z* 469.2 $[M+H]^+$; purity (LC-MS): 96%, t_R = 2.61 min.

1-((4-trifluoromethyl)benzyl)-2-(3-((*N*,*N*-diethylamino)methyl)-2-hydroxyanilino)benzo[*d*]imidazole (24): Brown semi-solid (105 mg, 70% yield); ^{1}H NMR (400 MHz, MeOH-d_4) δ 7.77 (dd, *J* = 2.2, 7.2 Hz, 1H), 7.59 (d, *J* = 8.0 Hz, 2H), 7.44-7.40 (m, 1H), 7.38 (d, *J* = 8.0 Hz, 2H), 7.19-7.15 (m, 1H), 7.11 (td, *J* = 7.6, 1.3 Hz, 1H), 7.05 (td, *J* = 7.5, 1.1 Hz, 1H), 6.77-6.67 (m, 2H), 5.46 (s, 2H), 3.81 (s, 2H), 2.64 (q, *J* = 7.2 Hz, 4H), 1.09 (t, *J* = 7.1 Hz, 6H); ^{13}C NMR (101 MHz, MeOH-d_4) δ 152.4, 150.4, 142.6, 142.0, 135.1, 131.1, 129.3, 128.6 (2C), 126.8 (2C),

125.5, 123.8, 122.9, 122.5, 121.9, 120.0, 119.3, 117.4, 109.4, 57.6, 47.4 (2C), 46.3 and 11.3 (2C); LC-MS (ESI): *m/z* 469.2 $[M+H]^+$; purity (LC-MS): 98%, t_R = 2.65 min.

1-((4-trifluoromethyl)benzyl)-2-(3-((*N*,*N*-diethylamino)methyl)-2-hydroxy-5-methylanilino)benzo[*d*]imidazole (25): Brown solid (120 mg, 46% yield); ^{1}H NMR (400 MHz, MeOH-d_4) δ 7.65 – 7.53 (m, 3H), 7.46 – 7.42 (m, 1H), 7.40 – 7.34 (m, 2H), 7.21 – 7.16 (m, 1H), 7.11 (td, *J* = 1.4, 7.6 Hz, 1), 7.05 (td, *J* = 1.2, 7.6 Hz, 1H), 6.59 – 6.49 (m, 1H), 5.44 (s, 2H), 3.75 (s, 2H), 2.63 (q, *J* = 7.2 Hz, 4H), 2.23 (s, 3H), 1.07 (t, *J* = 7.2 Hz, 6H); ^{13}C NMR (101 MHz, MeOH-d_4) δ 152.4, 147.5, 142.6, 142.0, 135.1, 131.2, 128.9, 128.8, 128.6 (2C), 126.8 (2C), 125.5, 124.3, 123.0, 122.5, 121.9, 120.6, 117.4, 109.3, 57.5, 47.5 (2C), 46.3, 21.0, 11.4 (2C); LC-MS (ESI): *m/z* = 483.2 $[M+H]^+$; purity (LC-MS): 98%, t_R = 2.68 min.

1-((4-trifluoromethyl)benzyl)-2-(3-((*N*,*N*-diethylamino)methyl)-2-hydroxy-6-methylanilino)benzo[*d*]imidazole (26): Brown semi-solid (96 mg, 62% yield); ^{1}H NMR (600 MHz, MeOH-d_4) δ 7.61 (d, *J* = 8.2 Hz, 2H), 7.43 (d, *J* = 8.1 Hz, 2H), 7.26-7.23 (m, 1H), 7.08-7.05 (m, 1H), 7.02 (td, *J* = 7.6, 1.2 Hz, 1H), 6.97 (td, *J* = 7.5, 1.1 Hz, 1H), 6.86 (d, *J* = 7.7 Hz, 1H), 6.67 (d, *J* = 7.7 Hz, 1H), 5.49 (s, 2H), 3.82 (s, 2H), 2.68 (q, *J* = 7.1 Hz, 4H), 2.11 (s, 3H), 1.09 (t, *J* = 7.1 Hz, 6H); ^{13}C NMR (151 MHz, MeOH-d_4) δ 155.2, 154.5, 142.5, 142.4, 137.3, 135.4, 130.7, 128.6 (2C), 127.6, 126.6 (2C), 125.5, 124.7, 122.6, 121.5, 121.2, 121.1, 116.4, 109.1, 57.1, 47.4 (2C), 46.2, 18.3 and 11.2 (2C); LC-MS (ESI): *m/z* 483.2 $[M+H]^+$; purity (LC-MS): 98%, t_R = 2.64 min.

1-(4-fluorobenzyl)-2-(3-((*N*,*N*-diethylamino)methyl)-4-hydroxyanilino)benzo[*d*]imidazole (27): Pink semi-solid (146 mg, 91% yield); ^{1}H NMR (600 MHz, MeOH-d_4) δ 7.64 (d, *J* = 2.6 Hz, 1H), 7.46-7.44 (m, 1H), 7.43 (dd, *J* = 2.6, 8.6 Hz, 1H), 7.36 (dd, *J* = 5.2, 8.5 Hz, 2H), 7.35-7.32 (m, 1H), 7.26

(td, *J* = 7.7, 1.4 Hz, 1H), 7.23 (td, *J* = 7.6, 1.3 Hz), 7.11 (t, *J* = 8.7 Hz, 2H), 7.07 (d, *J* = 8.6 Hz, 1H), 5.55 (s, 2H), 4.34 (s, 2H), 3.27 (q, *J* = 7.2 Hz, 4H), 1.40 (t, *J* = 7.2 Hz, 6H); ^{13}C NMR (151 MHz, MeOH-d_4) δ 163.9, 156.8, 151.2, 133.6, 132.9, 132.0, 130.1 (2C), 129.9, 129.8, 129.0, 124.9, 124.3, 118.9, 117.9, 116.9 (2C), 114.3, 111.3, 52.2, 48.6 (2C), 46.6 and 9.1 (2C); LC-MS (ESI): *m/z* 419.2 $[M+H]^+$; purity (LC-MS): 98%, t_R = 2.41 min.

1-(4-fluorobenzyl)-2-(4-((*N*,*N*-diethylamino)methyl)-3-hydroxyanilino)benzo[*d*]imidazole (28): Brown semi-solid (102 mg, 63% yield); ^{1}H NMR (600 MHz, MeOH-d_4) δ 7.41-7.38 (m, 1H), 7.16 (dd, *J* = 5.3, 8.5 Hz, 2H), 7.13-7.10 (m, 1H), 7.08 (td, *J* = 7.7, 1.1 Hz, 1H), 7.03 (td, *J* = 7.7, 1.1 Hz, 1H), 7.00 (t, *J* = 8.7 Hz, 2H), 6.95-6.84 (m, 3H), 5.37 (s, 2H), 3.74 (s, 2H), 2.63 (q, *J* = 7.2 Hz, 4H), 2.10 (s, 3H), 1.10 (t, *J* = 7.1 Hz, 6H); ^{13}C NMR (151 MHz, MeOH-d_4) δ 163.6, 160.0, 152.3, 142.5, 134.9, 133.8, 131.6, 130.1, 129.7 (2C), 122.9, 121.9, 117.8, 117.3, 116.5 (2C), 111.2, 109.8, 108.1, 57.1, 47.3 (2C), 46.0 and 11.6 (2C); LC-MS (ESI): *m/z* 419.2 $[M+H]^+$; purity (LC-MS): 98%, t_R = 2.52 min.

1-(4-fluorobenzyl)-2-(3-((*N*,*N*-diethylamino)methyl)-2-hydroxyanilino)benzo[*d*]imidazole (29): Brown semi-solid (112 mg, 70% yield); ^{1}H NMR (400 MHz, MeOH-d_4) δ 7.77 (dd, *J* = 2.2, 7.3 Hz, 1H), 7.44-7.40 (m, 1H), 7.27 (dd, *J* = 5.2, 8.6 Hz, 2H), 7.25-7.21 (m, 1H), 7.13-7.06 (m, 2H), 7.03 (t, *J* = 8.7 Hz, 2H), 6.77-6.69 (m, 2H), 5.36 (s, 2H), 3.84 (s, 2H), 2.69 (q, *J* = 7.2 Hz, 4H), 1.12 (t, *J* = 7.2 Hz, 6H); ^{13}C NMR (101 MHz, MeOH-d_4) δ 163.8, 152.2, 150.1, 142.6, 135.1, 133.4, 130.0 (2C), 129.4, 123.6, 122.8, 122.5, 121.9, 119.5, 119.3, 117.4, 116.7 (2C), 109.4, 57.6, 47.5 (2C), 46.1 and 11.3 (2C); LC-MS (ESI): *m/z* 419.2 $[M+H]^+$; purity (LC-MS): 98%, t_R = 2.55 min.

1-(4-fluorobenzyl)-2-(3-((*N*,*N*-diethylamino)methyl)-2-hydroxy-5-methylanilino)benzo[*d*]imidazole (30): Yellow semi-solid (140 mg, 84% yield); ^{1}H NMR (400 MHz, MeOH-d_4) δ 7.61 (d, *J* = 2.0 Hz, 1H), 7.45-7.41 (d, *J* = 7.5 Hz, 1H), 7.24 (dd, *J* = 5.3, 8.6 Hz, 2H), 7.22-7.19 (m, 1H), 7.14-7.06 (m, 2H), 7.03 (t, *J* = 8.7 Hz, 2H), 6.53 (d, *J* = 2.0 Hz, 1H), 5.32 (s, 2H), 3.77 (s, 2H), 2.65 (q, *J* = 7.2 Hz, 4H), 2.24 (s, 3H), 1.09 (t, *J* = 7.2 Hz, 6H); ^{13}C NMR (101 MHz, MeOH-d_4) δ 163.8, 152.2, 147.2, 142.5, 135.1, 133.4, 130.0 (2C), 129.0, 128.9, 124.2, 122.8, 122.4, 121.9, 120.2, 117.4, 116.7 (2C), 109.4, 57.5, 47.5 (2C), 46.1, 21.0 and 11.4 (2C); LC-MS (ESI): *m/z* 433.2 $[M+H]^+$; purity (LC-MS): 98%, t_R = 2.61 min.

1-(4-fluorobenzyl)-2-(3-((*N*,*N*-diethylamino)methyl)-2-hydroxy-6-methylanilino)benzo[*d*]imidazole (31): Brown semi-solid (112 mg, 68% yield); ^{1}H NMR (600 MHz, MeOH-d_4) δ 7.31 (dd, *J* = 5.3, 8.6 Hz, 2H), 7.24-7.21 (d, *J* = 7.8 Hz, 1H), 7.10-7.07 (d, *J* = 8.1 Hz, 1H), 7.03 (t, *J* = 8.7 Hz, 2H), 7.00 (td, *J* = 7.5, 1.3 Hz, 1H), 6.96 (td, *J* = 7.5, 1.1 Hz, 1H), 6.85 (d, *J* = 7.7 Hz, 1H), 6.67 (d, *J* = 7.7 Hz, 1H), 5.37 (s, 2H), 3.81 (s, 2H), 2.66 (q, *J* = 7.2 Hz, 4H), 2.10 (s, 3H), 1.09 (t, *J* = 7.1 Hz, 6H); ^{13}C NMR (151 MHz, MeOH-d_4) δ 163.7, 155.2, 154.5, 142.4, 137.1, 135.5, 133.9, 130.0 (2C), 127.4, 126.7, 122.4, 121.5, 121.3, 121.1, 116.5 (2C), 116.4, 109.2, 57.3, 47.3 (2C), 45.9, 18.3 and 11.4 (2C); LC-MS (ESI): *m/z* 433.2 $[M+H]^+$; purity (LC-MS): 98%, t_R = 2.51 min.

2-((*N*-ethylamino)methyl)-4-methyl-6-((1-(4-(trifluoromethyl)benzyl)-1H-benzo[*d*]imidazol-2-yl)amino)phenol (32): Brown solid (56 mg, 34% yield); ^{1}H NMR (600 MHz, MeOH-d_4) δ 7.62 (d, *J* = 8.1 Hz, 2H), 7.55 – 7.51 (m, 1H), 7.46 – 7.37 (m, 3H), 7.17 – 7.21 (m, 1H), 7.12 (td, *J* = 1.2, 7.6 Hz, 1H), 7.06 (td, *J* = 1.1, 7.6 Hz, 1H), 6.64 – 6.59 (m, 1H), 5.51 (s, 2H), 3.96 (s, 2H), 2.78 (q, *J* = 7.2 Hz, 2H), 2.24 (s, 3H), 1.18 (t, *J* = 7.2 Hz, 3H); ^{13}C NMR (151 MHz, MeOH-d_4) δ 152.5, 149.8, 142.5,

142.1, 135.1, 130.9, 129.8, 128.5 (2C), 127.4, 126.9 (2C), 125.5, 125.1, 123.0, 122.5, 121.9, 120.9, 117.2, 109.3, 51.6, 46.2, 43.3, 20.9, 13.6; LC-MS (ESI): *m/z* = 455.2 $[M+H]^+$; purity (LC-MS): 98%, t_R = 2.54 min.

2-((*N*-*tert*-butylamino)methyl)-4-methyl-6-((1-(4-(trifluoromethyl)benzyl)-1H-benzo[*d*]imidazol-2-yl)amino)phenol (33): Brown solid (58 mg, 38% yield); ^{1}H NMR (400 MHz, MeOH-d_4) δ 7.63 (d, *J* = 8.1 Hz, 2H), 7.45 – 7.36 (m, 3H), 7.18 (dd, *J* = 1.1, 8.1 Hz, 1H), 7.12 (td, *J* = 1.3, 7.6 Hz, 1H), 7.06 (td, *J* = 1.2, 7.6 Hz, 1H), 6.75 (d, *J* = 2.1 Hz, 1H), 5.53 (s, 2H), 4.06 (s, 2H), 2.25 (s, 3H), 1.36 (s, 9H); ^{13}C NMR (101 MHz, MeOH-d_4) δ 152.7, 149.6, 142.2, 142.1, 135.1, 130.9, 130.0, 128.4 (2C), 128.3, 126.9 (2C), 126.0, 125.5, 123.1, 122.5, 122.2, 122.0, 117.0, 109.5, 55.7, 46.3, 45.0, 26.9 (3C), 20.8; LC-MS (ESI): *m/z* = 483.2 $[M+H]^+$; purity (LC-MS): 98%, t_R = 2.58 min.

4-chloro-2-((*N*,*N*-diethylamino)methyl)-6-((1-(4-(trifluoromethyl)benzyl)-1H-benzo[*d*]imidazol-2-yl)amino)phenol (34): Brown solid (40 mg, 32% yield); ^{1}H NMR (600 MHz, MeOH-d_4) δ 7.81 (s, 1H), 7.62 (d, *J* = 8.1 Hz, 2H), 7.46 (d, *J* = 7.7 Hz, 1H), 7.39 (d, *J* = 8.1 Hz, 2H), 7.23 (d, *J* = 7.8 Hz, 1H), 7.15 (t, *J* = 7.4 Hz, 1H), 7.10 (t, *J* = 7.5 Hz, 1H), 6.80 (s, 1H), 5.52 (s, 2H), 3.94 (s, 2H), 2.82 (q, *J* = 7.2 Hz, 4H), 1.18 (t, *J* = 7.2 Hz, 6H); ^{13}C NMR (151 MHz, MeOH-d_4) δ 151.7, 149.5, 141.9, 141.7, 134.9, 131.1 (2C), 128.5 (3C), 126.9 (2C), 125.5, 123.7, 123.2, 122.7, 122.3, 119.9, 117.3, 109.6, 56.4, 47.8 (2C), 46.3, 10.7 (2C); LC-MS (ESI): *m/z* = 503.1 $[M+H]^+$; purity (LC-MS): 98%, t_R = 2.59 min.

4-chloro-2-((*N*-ethylamino)methyl)-6-((1-(4-(trifluoromethyl)benzyl)-1H-benzo[*d*]imidazol-2-yl)amino)phenol (35): Brown solid (40 mg, 35% yield); ^{1}H NMR (600 MHz, $CDCl_3$) δ 7.99 (s, 1H), 7.52 (dd, *J* = 7.7, 15.8 Hz, 3H), 7.30 (d, *J* = 7.9 Hz, 2H), 7.20 – 7.12 (m, 1H), 7.12 – 7.02 (m, 2H),

6.59 (s, 1H), 5.33 (s, 2H), 3.89 (s, 2H), 2.76 (q, *J* = 7.1 Hz, 2H), 1.18 (t, *J* = 6.8 Hz, 3H); ^{13}C NMR (151 MHz, $CDCl_3$) δ 149.6, 145.6, 140.6, 139.4, 133.5, 130.2, 129.7, 127.1 (2C), 126.7, 126.0 (2C), 125.5, 122.2, 122.1, 121.5, 121.2, 118.6, 116.9, 108.0, 50.2, 45.6, 42.8, 13.3; LC-MS (ESI): *m/z* = 475.1 $[M+H]^+$; purity (LC-MS): 98%, t_R = 2.56 min.

2-((*N*-*tert*-butylamino)methyl)-4-chloro-6-((1-(4-(trifluoromethyl)benzyl)-1H-benzo[*d*]imidazol-2-yl)amino)phenol (36): Brown solid (40 mg, 36% yield); ^{1}H NMR (600 MHz, MeOH-d_4) δ 7.99 (d, *J* = 2.6 Hz, 1H), 7.65 – 7.60 (m, 2H), 7.50 – 7.47 (m, 1H), 7.42 – 7.38 (m, 2H), 7.23 – 7.20 (m, 1H), 7.14 (td, *J* = 1.2, 7.6 Hz, 1H), 7.08 (td, *J* = 1.1, 7.6 Hz, 1H), 6.78 (d, *J* = 2.6 Hz, 1H), 5.52 (s, 2H), 4.04 (s, 2H), 1.35 (s, 9H); ^{13}C NMR (151 MHz, MeOH-d_4) δ 153.7, 151.5, 142.6, 142.0, 134.9, 132.4, 131.4, 128.4 (2C), 126.9 (2C), 125.5, 123.2, 123.1, 122.1, 121.0, 120.2, 118.3, 117.5, 109.3, 55.9, 46.2, 45.1, 26.6 (3C); LC-MS (ESI): *m/z* = 503.1 $[M+H]^+$; purity (LC-MS): 98%, t_R = 2.54 min.

2-((*N*,*N*-diethylamino)methyl)-4-fluoro-6-((1-(4-(trifluoromethyl)benzyl)-1H-benzo[*d*]imidazol-2-yl)amino)phenol (37): Brown solid (45 mg, 35% yield); ^{1}H NMR (600 MHz, MeOH-d_4) δ 7.73 (dd, *J* = 3.0, 10.6 Hz, 1H), 7.63 (d, *J* = 8.1 Hz, 2H), 7.51 (d, *J* = 7.8 Hz, 1H), 7.41 (d, *J* = 8.1 Hz, 2H), 7.27 (d, *J* = 7.8 Hz, 1H), 7.19 – 7.15 (m, 1H), 7.15 – 7.10 (m, 1H), 6.49 (dd, *J* = 2.9, 8.7 Hz, 1H), 5.52 (s, 2H), 3.83 (s, 2H), 2.70 (q, *J* = 7.2 Hz, 4H), 1.13 (t, *J* = 7.2 Hz, 6H); ^{13}C NMR (151 MHz, MeOH-d_4) δ 157.6, 151.4, 145.5, 141.9, 135.0, 131.2, 128.6 (2C), 127.9, 126.9 (2C), 125.5, 123.1 (2C), 122.3 (2C), 117.7, 109.5, 108.8, 106.1, 57.3, 47.6 (2C), 46.3, 11.3 (2C); LC-MS (ESI): *m/z* = 487.2 $[M+H]^+$; purity (LC-MS): 98%, t_R = 2.53 min.

3-chloro-2-((*N*,*N*-diethylamino)methyl)-6-((1-(4-(trifluoromethyl)benzyl)-1H-benzo[*d*]imidazol-2-yl)amino)phenol (38): Brown solid (40 mg, 34% yield); ^{1}H NMR (600 MHz, MeOH-d_4) δ 7.82 (d, *J* = 8.6 Hz, 1H), 7.63 (d, *J* = 8.0 Hz, 2H), 7.48 – 7.43 (m, 1H), 7.41 (d, *J* = 8.0 Hz, 2H), 7.25 – 7.20 (m, 1H), 7.15 (td, *J* = 1.2, 7.6 Hz, 1H), 7.10 (td, *J* = 1.1, 7.6 Hz, 1H), 6.77 (d, *J* = 8.7 Hz, 1H), 5.51 (s, 2H), 4.15 (s, 2H), 2.84 (q, *J* = 7.1 Hz, 4H), 1.19 (t, *J* = 7.2 Hz, 6H); ^{13}C NMR (151 MHz, MeOH-d_4) δ 153.7, 152.0, 142.4, 142.0, 135.0, 130.9, 129.0, 128.5 (2C), 127.7, 126.9 (2C), 125.5, 123.0, 122.1, 120.2, 118.4, 118.3, 117.4, 109.4, 54.4, 47.8 (2C), 46.3, 10.8 (2C); LC-MS (ESI): *m/z* = 503.1 $[M+H]^+$; purity (LC-MS): 98%, t_R = 2.59 min.

2-((5,6-difluoro-1-(4-(trifluoromethyl)benzyl)-1H-benzo[d]imidazol-2-yl)amino)-6-((*N*-ethylamino)methyl)-4-methylphenol (39): Brown solid (47 mg, 56% yield); ^{1}H NMR (600 MHz, MeOH-d_4) δ 7.64 (d, *J* = 8.1 Hz, 2H), 7.45 (d, *J* = 2.1 Hz, 1H), 7.39 (d, *J* = 8.0 Hz, 2H), 7.22 (dd, *J* = 7.2, 10.8 Hz, 1H), 7.14 (dd, *J* = 7.0, 10.2 Hz, 1H), 6.70 (d, *J* = 2.0 Hz, 1H), 5.48 (s, 2H), 4.01 (s, 2H), 2.84 (q, *J* = 7.2 Hz, 2H), 2.23 (s, 3H), 1.21 (t, *J* = 7.2 Hz, 3H); ^{13}C NMR (151 MHz, MeOH-d_4) δ 154.1, 149.7, 148.3, 147.6, 146.8, 138.0, 131.3, 130.7, 129.3, 128.4 (2C), 128.0, 126.9 (2C), 126.2, 125.5, 122.4, 122.3, 105.0, 98.3, 50.9, 46.5, 43.4, 20.8, 13.1; LC-MS (ESI): *m/z* = 491.1 $[M+H]^+$; purity (LC-MS): 98%, t_R = 2.57 min.

2-((*N*-*tert*-butylamino)methyl)-6-((5,6-difluoro-1-(4-(trifluoromethyl)benzyl)-1H-benzo[*d*]imidazol-2-yl)amino)-4-methylphenol (40): Brown solid (57 mg, 47% yield); ^{1}H NMR (600 MHz, $CDCl_3$) δ 7.81 (s, 1H), 7.59 (d, *J* = 8.0 Hz, 2H), 7.33 (m, 3H), 6.84 (dd, *J* = 6.8, 9.7 Hz, 1H), 6.48 (s, 1H), 5.37 (s, 2H), 3.90 (s, 2H), 2.16 (s, 3H), 1.28 (s, 9H); ^{13}C NMR (151 MHz, $CDCl_3$) δ 151.3, 147.3, 146.4, 143.8, 138.9, 136.8, 130.6, 128.9, 128.0, 126.2 (2C), 126.1 (2C), 125.5, 124.7, 123.1,

122.9, 121.5, 105.2, 96.5, 52.9, 46.0, 45.1, 27.8 (3C), 20.9; LC-MS (ESI): *m/z* = 519.2 $[M+H]^+$; purity (LC-MS): 98%, t_R = 2.60 min.

4-chloro-2-((5,6-difluoro-1-(4-(trifluoromethyl)benzyl)-1H-benzo[*d*]imidazol-2-yl)amino)-6-((*N*-ethylamino)methyl)phenol (41): Brown solid (45 mg, 36% yield); ^{1}H NMR (600 MHz, $CDCl_3$) δ 8.09 (s, 1H), 7.41 (d, *J* = 8.0 Hz, 2H) 7.15 (m, 3H), 6.65 (dd, *J* = 6.9, 9.4 Hz, 1H), 6.39 (s, 1H), 5.02 (s, 2H), 3.71 (s, 2H), 2.51 (q, *J* = 7.2 Hz, 2H), 0.96 (t, *J* = 7.2 Hz, 3H); ^{13}C NMR (151 MHz, $CDCl_3$) δ 150.2, 147.4, 146.5, 144.8, 138.5, 137.1, 130.8, 128.9, 127.1 (2C), 126.5, 126.3 (2C), 125.5, 123.9, 121.8, 120.9, 116.7, 105.7, 96.3, 51.5, 46.1, 43.0, 14.4; LC-MS (ESI): *m/z* = 511.2 $[M+H]^+$; purity (LC-MS): 98%, t_R = 2.60 min.

2-((*N*-*tert*-butylamino)methyl)-4-chloro-6-((5,6-difluoro-1-(4-(trifluoromethyl)benzyl)-1H-benzo[*d*]imidazol-2-yl)amino)phenol (42): Brown solid (44 mg, 37% yield); ^{1}H NMR (600 MHz, $CDCl_3$) δ 8.36 – 8.23 (m, 1H), 7.62 (d, *J* = 8.1 Hz, 2H), 7.37 (dd, *J* = 8.6, 24.1 Hz, 3H), 6.86 (t, *J* = 8.2 Hz, 1H), 6.62 (d, *J* = 2.5 Hz, 1H), 5.26 (s, 2H), 3.91 (s, 2H), 1.24 (s, 9H); ^{13}C NMR (151 MHz, $CDCl_3$) δ 150.3, 147.4, 146.5, 144.9, 138.6, 130.8, 129.1, 128.9 (2C), 127.2 (2C), 126.2 (2C), 125.5, 124.7, 123.9, 122.9, 122.6, 105.6, 96.4, 52.2, 46.2, 45.3, 28.1 (3C); LC-MS (ESI): *m/z* = 539.1 $[M+H]^+$; purity (LC-MS): 98%, t_R = 2.61 min.

2-((1H-benzo[d]imidazol-2-yl)amino)-6-((*N*-*tert*-butylamino)methyl)-4-methylphenol (43): Brown solid (22 mg, 43% yield); ^{1}H NMR (600 MHz, MeOH-d_4) δ 7.29 (dd, *J* = 3.2, 5.8 Hz, 2H), 7.11 – 7.09 (m, 1H), 7.05 (dd, *J* = 3.2, 5.9 Hz, 2H), 6.97 – 6.95 (m, 1H), 4.16 (s, 2H), 2.28 (s, 3H), 1.46 (s, 9H); ^{13}C NMR (151 MHz, MeOH-d_4) δ 153.6, 146.9, 138.2, 130.7, 129.7, 128.1, 124.9, 122.9, 122.3

(4C), 113.5, 58.0, 43.5, 26.1 (3C), 20.5; LC-MS (ESI): *m/z* = 325.2 $[M+H]^+$; purity (LC-MS): 98%, t_R = 2.06 min.

2-((1H-benzo[*d*]imidazol-2-yl)amino)-4-chloro-6-((*N*-ethylamino)methyl)phenol (44): Brown solid (38 mg, 50% yield); ^{1}H NMR (600 MHz, MeOH-d_4) δ 7.34 (d, *J* = 2.5 Hz, 1H), 7.31 (dd, *J* = 3.2, 5.9 Hz, 2H), 7.12 (d, *J* = 2.5 Hz, 1H), 7.07 (dd, *J* = 3.1, 5.9 Hz, 2H), 4.19 (s, 2H), 3.11 (q, *J* = 7.3 Hz, 2H), 1.35 (t, *J* = 7.3 Hz, 3H); ^{13}C NMR (151 MHz, MeOH-d_4) δ 152.8, 148.1, 137.6, 131.5, 126.6, 124.9, 123.9, 123.3, 122.6 (4C), 113.7, 48.1, 43.8, 11.5; LC-MS (ESI): *m/z* = 317.1 $[M+H]^+$; purity (LC-MS): 98%, t_R = 0.67 min.

2-((1H-benzo[d]imidazol-2-yl)amino)-6-((*N*-*tert*-butylamino)methyl)-4-chlorophenol (45): Brown solid (13 mg, 25% yield); ^{1}H NMR (600 MHz, MeOH-d_4) δ 7.76 (d, *J* = 2.6 Hz, 1H), 7.31 (dd, *J* = 3.2, 5.8 Hz, 2H), 7.05 (dd, *J* = 3.2, 5.9 Hz, 2H), 6.87 (d, *J* = 2.6 Hz, 1H), 4.09 (s, 2H), 1.39 (s, 9H); ^{13}C NMR (151 MHz, MeOH-d_4) δ 152.6, 151.3, 138.4, 132.1, 123.7, 122.7, 122.1 (5C), 119.4, 113.6, 56.1, 44.7, 26.7 (3C); LC-MS (ESI): *m/z* = 345.1 $[M+H]^+$; purity (LC-MS): 98%, t_R = 2.18 min.

2-((1H-benzo[d]imidazol-2-yl)amino)-4-(tert-butyl)-6-((*N*-*tert*-butylamino)methyl)phenol (46): Brown solid (20 mg, 39% yield); ^{1}H NMR (600 MHz, MeOH-d_4) δ 7.30 (d, *J* = 2.4 Hz, 1H), 7.29 (dd, *J* = 3.2, 5.8 Hz, 2H), 7.20 (d, *J* = 2.4 Hz, 1H), 7.05 (dd, *J* = 3.1, 5.9 Hz, 2H), 4.21 (s, 2H), 1.47 (s, 9H), 1.33 (s, 9H); ^{13}C NMR (151 MHz, MeOH-d_4) δ 153.7, 146.9, 144.2, 138.2, 129.3, 124.7, 122.6, 122.3 (4C), 121.6, 131.5, 58.0, 43.9, 35.0, 31.9 (3C), 26.1 (3C); LC-MS (ESI): *m/z* = 367.2 $[M+H]^+$; purity (LC-MS): 98%, t_R = 2.35 min.

2-((*N*-*tert*-butylamino)methyl)-6-((5,6-difluoro-1H-benzo[*d*]imidazol-2-yl)amino)-4-methylphenol (47): Brown solid (20 mg, 35% yield); ^{1}H NMR (600 MHz, MeOH-d_4) δ 7.19 (d, *J* = 2.1 Hz, 1H), 7.16 – 7.12 (m, 2H), 6.91 (d, *J* = 2.0 Hz, 1H), 4.13 (s, 2H), 2.28 (s, 3H), 1.43 (s, 9H); ^{13}C NMR (151 MHz, MeOH-d_4) δ 155.0, 147 (3C), 134.0, 130.1, 129.4, 127.6 (2C), 124.3, 122.8, 101.7, 101.6, 57.3, 43.9, 26.4 (3C), 20.6; LC-MS (ESI): *m/z* = 361.1 $[M+H]^+$; purity (LC-MS): 98%, t_R = 2.33 min.

4-chloro-2-((5,6-difluoro-1H-benzo[*d*]imidazol-2-yl)amino)-6-((*N*-ethylamino)methyl)phenol (48): Brown solid (33 mg, 39% yield); ^{1}H NMR (600 MHz, MeOH-d_4) δ 7.47 (d, *J* = 2.5 Hz, 1H), 7.23 – 7.17 (m, 2H), 7.12 (d, *J* = 2.4 Hz, 1H), 4.21 (s, 2H), 3.12 (q, *J* = 7.3 Hz, 2H), 1.37 (t, *J* = 7.3 Hz, 3H); ^{13}C NMR (151 MHz, MeOH-d_4) δ 154.2, 148.2, 148.1 (2C), 147.1, 133.6, 131.3, 126.3 (2C), 124.9, 123.7, 122.9, 101.9, 48.3, 43.8, 11.6; LC-MS (ESI): *m/z* = 353.1 $[M+H]^+$; purity (LC-MS): 98%, t_R = 2.30 min.

2-((*N*-*tert*-butylamino)methyl)-4-chloro-6-((5,6-difluoro-1H-benzo[*d*]imidazol-2-yl)amino)phenol (49): Brown solid (21 mg, 37% yield); ^{1}H NMR (600 MHz, MeOH-d_4) δ 7.86 (d, *J* = 2.6 Hz, 1H), 7.19 – 7.13 (m, 2H), 6.81 (d, *J* = 2.5 Hz, 1H), 4.06 (s, 2H), 1.36 (s, 9H); ^{13}C NMR (151 MHz, MeOH-d_4) δ 154.0, 152.2, 148.2 (2C), 134.2, 131.9, 123.4 (2C), 122.2, 121.3, 118.7 (2C), 101.7, 55.7, 45.1, 26.8 (3C); LC-MS (ESI): *m/z* = 381.1 $[M+H]^+$; purity (LC-MS): 98%, t_R = 2.39 min.

4-(*tert*-butyl)-2-((tert-butylamino)methyl)-6-((5,6-difluoro-1H-benzo[*d*]imidazol-2-yl)amino)phenol (50): Brown solid (19 mg, 34% yield); ^{1}H NMR (600 MHz, MeOH-d_4) δ 7.35 (d, *J* = 2.4 Hz, 1H), 7.18 (d, *J* = 2.4 Hz, 1H), 7.16 – 7.12 (m, 2H), 4.18 (s, 2H), 1.45 (s, 9H), 1.32 (s, 9H); ^{13}C NMR (151 MHz, MeOH-d_4) δ 155.2, 148.0 (2C), 147.6, 144.0, 134.0, 128.9, 124.7 (2C), 122.5,

121.6 (2C), 101.7, 57.6, 44.0, 35.1, 31.9 (3C), 26.3 (3C); LC-MS (APCI/ESI): *m/z* = 403.2 $[M+H]^+$; purity (LC-MS): 98%, t_R = 2.48 min.

2-((*N-tert*-butylamino)methyl)-6-((4,6-dichloro-1H-benzo[*d*]imidazol-2-yl)amino)-4-methylphenol (51): Brown solid (22 mg, 36% yield); ^{1}H NMR (600 MHz, MeOH-d_4) δ 7.28 – 7.26 (m, 1H), 7.21 (d, *J* = 1.8 Hz, 1H), 7.06 (d, *J* = 1.8 Hz, 1H), 6.87 (d, *J* = 2.1 Hz, 1H), 4.11 (s, 2H), 2.27 (s, 3H), 1.41 (s, 9H); ^{13}C NMR (151 MHz, MeOH-d_4) δ 154.9, 148.1, 139.7, 135.8, 129.7, 129.2, 127.4, 127.2, 123.9, 122.9, 121.6, 119.0, 112.0, 57.0, 44.1, 26.4 (3C), 20.6; LC-MS (ESI): *m/z* = 393.1 $[M+H]^+$; purity (LC-MS): 98%, t_R = 2.50 min.

2-(aminomethyl)-4-methyl-6-((1-(4-(trifluoromethyl)benzyl)-1H-benzo[d]imidazol-2-yl)amino)phenol (52): Intermediate III was synthesized from 3 and 2-amino-4-methylphenol (8d) (Scheme 1) according to general synthetic procedure V, followed by a Mannich reaction with 4-methoxy benzylamine (PMB, 1.2 eq) in ethanol in the presence of formaldehyde (1.2 eq). The reaction lasted for 16 h for complete consumption of starting materials, followed by an acid work-up (1M HCl) to obtain crude product, which was purified by flash chromatography. Compound 52 was obtained by cleavage of the PMB group in the presence of trifluoroacetic acid in DCM at room temperature for 48 h, followed by purification by flash chromatography. Brown solid (13 mg, 28% yield); ^{1}H NMR (600 MHz, MeOH-d_4) δ 7.59 (d, *J* = 7.5 Hz, 2H), 7.39 (m, 3H), 7.34 (d, *J* = 7.8 Hz, 1H), 7.14 (d, *J* = 7.5 Hz, 1H), 7.10 (t, *J* = 7.4 Hz, 1H), 7.04 (t, *J* = 7.5 Hz, 1H), 6.72 (m, 1H), 5.47 (s, 2H), 3.97 (s, 2H), 2.24 (s, 3H). ^{13}C NMR (151 MHz, MeOH-d_4) δ 152.8, 149.4, 142.5, 142.1, 135.1, 131.0, 130.1, 128.3 (2C), 126.8 (2C), 126.4, 125.7, 125.6, 124.6, 123.1, 122.0, 121.9, 117.0, 109.5, 55.7, 46.2, 20.8; LC-MS (ESI): *m/z* = 427.1 $[M+H]^+$; purity (LC-MS): 98%, t_R = 2.45 min.

Antiplasmodium activity evaluation: Compounds were screened against multidrug resistant (K1) and sensitive (NF54) strains of *P. falciparum in vitro* using the modified [^{3}H]-hypoxanthine incorporation assay.[38] *In vivo* efficacy was conducted as previously described,[39] with the modification that mice (n= 3) were infected with a GFP-transfected *P. berghei* ANKA strain (donated by A. P. Waters and C. J. Janse, Leiden University, The Netherlands), and parasitemia was determined using standard flow cytometry techniques. The detection limit was 1 parasite in 1000erythrocytes (that is, 0.1%). Activity was calculated as the difference between the mean percent parasitemia for the control and treated groups expressed as a percent relative to the control group. Compounds were dissolved or suspended in a vehicle consisting of 70% Tween-80 and 30% ethanol, followed by a 10-fold dilution in H_2O and administered orally as four consecutive daily doses (4, 24, 48, and 72 h after infection). Blood samples for the quadruple-dose regimens were collected on day 4 (96 h after infection).

Gametocytocidal activity evaluation: The luciferase reporter assay[24] was established to enable accurate, reliable and quantifiable investigations of the stage-specific action of gametocytocidal compounds for the early and late gametocyte marker cell line NF54-PfS16-GFP-Luc. Drug assays were set up on day 5 and 10 (representing >90% of either early stage II/III or mature stage IV/V gametocytes, respectively). In each instance, assays were set up using a 2 – 3% gametocytemia, 1.5% hematocrit culture and 48 h drug pressure in a gas chamber (90% N_2, 5% O_2, and 5% CO_2) at 37 ºC. Luciferase activity was determined in 30 µL parasite lysates by adding 30 µL luciferin substrate (Promega Luciferase Assay System) at room temperature and detection of resultant bioluminescence at an integration constant of 10 s with the GloMax® Explorer Detection System with Instinct® Software. Methylene blue (5 µM) was used as a reference compound in the *in vitro*

gametocyte luciferase reporter assay as previously reported.[40] Dual point analysis was performed for a single biological replicate in technical triplicates. The IC_{50} was again determined using non-linear curve fit (GraphPad Prism V6.0) normalised to maximum and minimum inhibition and data are from at least three independent biological replicates, each performed in technical triplicates.

Male gamete exflagellation assay: The male gamete exflagellation inhibition assay (EIA)[41] was performed by treating mature (>90% stage V) gametocytes with 2 µM compound (10 mM stock solutions in 100% DMSO (w/v), Sigma-Aldrich) in complete culture media (final DMSO concentration of < 0.1% (v/v)) for 48 h at 37°C under 90% N_2, 5% CO_2, and 5% O_2 hypoxic conditions. Following treatment gametogenesis was induced with 100 µM xanthurenic acid (Sigma Aldrich) in ookinete medium (complete RPMI 1640 with 25 mM HEPES, 0.2% sodium bicarbonate, pH 8.0, and 20% human serum) at room temperature for 15 min. Exflagellating centers were detected by video microscopy (Carl Zeiss NT 6V/10W Stab480 microscope with a MicroCapture camera, 10X magnification) in a Neubauer chamber at RT and semi-automatically quantified after 20 min from 15 randomly located fields from which videos of 8-10 s each were taken at 30 s intervals. The total exflagellating centres per treatment were quantified using ICY (open-source imaging software GPLv3) normalised to an untreated control. Assays were performed for a single biological repeat.

SALI Plot analysis: Structure–activity landscape index (SALI) was performed using Osiris Datawarrior V 5.2.1 software (www.openmolecules.org). Compound similarity/activity cliff analysis was performed based on compound SMILES, taking stereochemistry into account, and separation based on compound neighbor at a similarity threshold of 86%.

Cytotoxicity evaluation: The *in vitro* cytotoxicity of the synthesized compounds was evaluated against the Chinese Hamster Ovarian (CHO) cancer cell line using the MTT [3-(4,5-dimethylthiazolyl-2)-2,5-diphenyltetrazolium bromide] assay, which is a colorimetric assay based on assessing the cell metabolic activity.[42]

The synthesized compounds were assayed in triplicate. Stock solutions of 2 mg/mL of test samples in DMSO were prepared with poorly soluble samples being tested as suspensions. The compounds were kept at -20 ^{o}C until required. In all experiments, emetine was used as a reference drug. Starting from an initial concentration of 100 µg/mL, ten-fold serial dilutions were made in complete medium to give 6 concentrations to the lowest concentration of 0.001 µg/mL. The cell viability was not affected by the highest concentration of the solvent to which the cells were exposed. The full dose-response curves were plotted using a non-linear dose-response curve fitting analysis via GraphPad Prism V4 software. By this, the minimum concentration required for 50% inhibition (IC_{50}) values were determined for each compound.

Caucasian hepatocellular carcinoma cells (HepG2) were maintained as previously described.[43] Cells were grown in Dulbecco's Modified Eagle's Medium (DMEM) (HyClone) supplemented with 5% Fetal Bovine Serum (heat inactivated) and 1% Penicillin/Streptomycin (Sigma-Aldrich) at 37 °C at 5% CO_2. Cell viability was monitored microscopically with 0.2% Trypan-Blue. Cells were trypsinised with 1x Trypsin-EDTA (Sigma) and ~100 000 cells were plated in 96-well plates and grown for 24 h. The cells were treated at treated with relevant compound and incubated for 48 h at 37 °C and 5% CO_2. Cytotoxicity was determined using the CytoSelect™ LDH Cytotoxicity Assay Kit (Cell Biolabs Inc., CBA-241) which was added to the supernatant. Absorbance was measured

at 450 nm. Data obtained were analyzed in Excel and experiments were performed in technical duplicates for three biological repeats (n=3).

In Vitro Hepatic Microsomal Stability: Metabolic stability studies were conducted in human, mouse and rat liver microsomes using a single-point (30-min) study design.[44] In brief, 1 µM of the compound was incubated with 0.4 mg/ml microsomes in 0.1M phosphate buffer pH 7.4. The reactions were quenched by the addition of ice-cold acetonitrile containing internal standard (carbamazepine, 0.0236 µg/mL). The samples were centrifuged, and the supernatant was analysed by means of LC-MS/MS (Agilent Rapid Resolution HPLC, AB SCIEX 4500 MS). The percentage compound remaining was calculated by using the internal standard corrected peak areas at 30 min, with those of the 0 min incubation. Propranolol, Midazolam and MMV390048 were used as assay controls.

Metabolite Identification Studies: The test compounds (10 µM) were incubated at 37 °C in a solution containing 1 mg/ml microsomes, magnesium chloride (5 mM) and NADPH (1 mM) in potassium phosphate buffer (100 mM, pH 7.4) for 60 minutes while shaking. The samples were then prepared by ice-cold acetonitrile precipitation, centrifuged, and filtered for LC-MS analysis. Controls containing all the sample constituents (not incubated), and in which NADPH, microsomes or the test compound were individually excluded, were also prepared, and handled similarly to the test sample. Verapamil (10 µM) was incubated concomitantly as a positive control. Metabolites formed in microsomal incubations were identified by comparison of the T60 chromatograms with chromatograms at T0 using Lightsight 2.3. The tentative identity of the metabolites was deduced by comparison of the product ion spectra of the $[M+H]^+$ ions of the metabolites with that of the parent compound using Analyst 1.6.3

Kinetic Solubility: Solubility was measured at pH 6.5 using an adapted miniaturised shake-flask method, in 96-well plate format.[45,46] Briefly 4 µl of a 10mM stock in DMSO was added to a 96-well plate and evaporated using a GeneVac system. Phosphate buffer pH 6.5 was then added to the wells and the plate was incubated for 24 h at 25 °C with shaking. At the end of this incubation, the samples were centrifuged at 3500 g for 15 min then transferred to an analysis plate. A calibration curve in DMSO for each sample between 10 – 220 µM was prepared and included in the analysis plate. Analysis was then performed by HPLC-DAD (Agilent Rapid Resolution HPLC with Diode array detector) and solubility of each sample determined from the corresponding calibration curve. Reserpine, Hydrocortisone, and MMV390048 were used as assay controls.

Pharmacokinetics: Male Balb/C mice were used for animal pharmacokinetic evaluations. All animal work was carried out in accordance with the University of Cape Town's ethics policies using protocols approved by the research ethics committee (AEC017/026). Compounds were administered intravenously as a bolus of DMA/PEG/PPG: 10/30/60 and orally in 0.5% (w/v) HPMC with 0.2% Tween80 aqueous solution to male Balb/C mice (n=3 for each group for 41 and for the oral group for 48 and n=5 for the intravenous group for 48). Mice were not fasted overnight and were allowed to eat *ad libitum*. Animals were permitted access *ad libitum* to water.

PK sampling: Blood samples were collected from the tail vein of the mice into heparinized microcentrifugation tubes at predetermined sampling times (0.17, 0.5, 1, 3, 5, 7, 9, and 24h for intravenous dosing; 0.5, 1, 3, 5, 7, 9 and 24h for oral dosing). All samples were stored at -80°C until extraction.

Bioanalytical method: Frozen whole blood was thawed at room temperature. 20 μL of samples were extracted by protein precipitation using 100 μL of acetonitrile containing 10 ng/ml of internal standard (MMV394902); and centrifuged. Calibration standards and quality controls were extracted following the same procedure. Supernatants were injected onto the column for LC-MS/MS analysis. The analytical limit of quantitation (LOQ) was 2 ng/mL. The accuracy, precision, and recovery for each study were within acceptable limits (Supplementary Information Table S2).

Calculation of pharmacokinetic parameters: PK parameters were calculated by non-compartmental analysis using PK Solutions 2.0 (Summit Research Services, Montrose, CO, USA) with a method based on curve stripping.

In Vitro Permeability: The PAMPA (Parallel Artificial Membrane Assay) assay was performed in triplicate in 96-well MultiScreen filter plates (Millipore, 0.4 μm PCTE membrane). Membrane filters were precoated with 5% hexadecane in hexane and allowed to dry prior to the assay. Membrane integrity marker, Lucifer yellow, was added to the apical wells of the precoated MultiScreen plate donor/ drug solutions containing test compound. Phosphate buffer (pH 7.4) was added to the 96-well acceptor plate. An amount of 10 mM test compound was used to spike (1 μM) the donor buffer at physiologically relevant pH values (4 and 6.5), and the donor plate was slotted into the acceptor plate and incubated (4 h at room temperature) with gentle shaking (40–50 rpm). Following incubation, samples from the acceptor wells and theoretical equilibrium wells were transferred to the analysis plate and matrix matched with blank donor buffer. Acetonitrile containing internal standard (carbamazepine, 0.0236 μg/mL) was added to all samples, and they were analyzed by LC–MS/MS (Agilent rapid resolution HPLC, AB SCIEX 4500

MS). The normalized (analyte/internal standard) peak areas were used to calculate the apparent permeability (Papp). Membrane integrity was assessed by calculating the Papp of Lucifer yellow (acceptable values < 50nm/s) using a Modulus microplate reader.[47,48]

β-hematin Inhibition: The inhibition of β-hematin formation assay was conducted to investigate the possible mechanism of antiplasmodium activity of the synthesized benzimidazole analogues as inhibitors of heme polymerization. This non-cell assay evaluates the ability of the test compounds to prevent the synthetic dimerization of hematin (β-hematin) in lipid medium.

Hundred microliters of a solution containing water/305.5 µM NP-40/DMSO at a v/v ratio of 70%/20%/10%, respectively, was added to every well in columns 2-12 of a 96-well plate. To column 1 was added 140 µL of water and 40 µL of 305.5 µM NP-40. Twenty microliters of the test compounds (20 mM), that is, the synthesized compounds and control, was added to column 1 in duplicate. One hundred microliters of the test solution were diluted to column 11, with column 12 left as a blank (0 µM of compound). A 178.8 µL aliquot of hematin (hemin) stock was suspended in 20 mL of a 1 M acetate buffer, pH 4.8 and 100 µL of this hematin suspension added into each well. Plates were then incubated for ~5 hours at 37 ^{o}C after which 32 µL of pyridine solution (20% water, 20% acetone, 10% 2M HEPES buffer (pH 7.4), 50% pyridine) was added followed by addition of 60 µL of acetone to all wells. Plates were again read at 405 nm on a Thermo Scientific Multiscan Go Microplate Spectrophotometer. The IC_{50} values were determined using GraphPad Prism 6.

Cell-based Heme Assay: Target validation was carried out through a cellular fractionation assay, optimized to a multi-well colorimetric assay for determining heme species in *P. falciparum* as

previously described.[49] The cellular fractionation allows the direct quantification of heme species in isolated trophozoites such as the freely exchangeable heme and hemozoin.

A two-tailed t-test (95% CI) was used for determination of statistical significance of differences in measurements relative to controls. The data represent a minimum of three repeats with standard deviations calculated for each of the average results. All the analysis was done using GraphPad Prism version 6.0.0 software.

Microtubule Inhibition: Asexual *Pf*NF54 parasites were maintained and early-stage gametocytes were induced and maintained as described above. Parasites were treated with 41 and 44 at 600 nM against asexual stages (~1% parasitaemia and 5% haematocrit, >95% D-sorbitol synchronized ring-stage culture) and 2400 nM against early stage (~2% gametocytaemia, 2% haematocrit 20% I/ 60% II/20% III) and incubated for 24 h at 37°C under 90% N_2, 5% CO_2, and 5% O_2 hypoxic conditions (final DMSO concentration of <0.1% (v/v)). Colchicine (20 µM) was used as a positive control with treated asexual parasites and early-stage gametocytes incubated for 24 h at 37°C under 90% N_2, 5% CO_2, and 5% O_2 hypoxic conditions. Following incubation parasites were stained with 250 nM Tubulin Tracker® Oregon Green 488, Taxol bis acetate (Invitrogen) for 30 min to visualize tubulin formation, and co-stained with the nuclear dye Hoechst 33324 (100 nM) for 10 min at 37°C under 90% N_2, 5% CO_2, and 5% O_2 hypoxic conditions in the dark. After staining cells were washed 3x with prewarmed PBS (137 mM NaCl, 2.7 mM KCl, 10 mM phosphate, pH 7.4) and visualized as live cells using a Zeiss LSM 510 Meta Confocal Microscope with Zeiss ZEN black software (Zeiss, Germany).

CONFLICT OF INTEREST

The authors declare no competing interest.

ACKNOWLEDGEMENTS

The University of Cape Town, South African Medical Research Council and South African Research Chairs Initiative of the Department of Science and Innovation, administered through the South African National Research Foundation (NRF, K.C. UID: 64767, LM.B. UID: 84627) and a NRF Community of Practice on 'Evaluating Malaria Control Interventions' (UID: 110666) are gratefully acknowledged for support. At Swiss TPH, we thank Sibylle Sax, Rahel Buehler, and Ursula Lehmann for assistance in performing antimalarial *in vitro* and *in vivo* assays.

ANCILLARY INFORMATION

Supplementary information file 1: Additional Experimental Results

Supplementary information file 2: Biological Results

Supplementary information file 3: Molecular Formula Strings

Corresponding author: kelly.chibale@uct.ac.za

Abbreviations Used: ABS, Asexual blood stage; EG, Early-stage gametocytes; LG, Late-stage gametocytes; TCP, Target candidate profile; TPP, Target product profile; RI, Resistance index; SI, Selective index; CHO, Chinese Hamster Ovarian cells; MLM, Mouse liver microsomes; RLM, Rat

liver microsomes; HLM, Human liver microsomes; βHIA, Beta hematin inhibition assay; SALI, Structure–activity landscape index.

REFERENCES

(1) *World Malaria Report 2020: 20 Years of Global Progress and Challenges.*; Geneva: World Health Organization; 2020.

(2) Uwimana, A.; Legrand, E.; Stokes, B. H.; Ndikumana, J.-L. M.; Warsame, M.; Umulisa, N.; Ngamije, D.; Munyaneza, T.; Mazarati, J.-B.; Munguti, K.; Campagne, P.; Criscuolo, A.; Ariey, F.; Murindahabi, M.; Ringwald, P.; Fidock, D. A.; Mbituyumuremyi, A.; Menard, D. Emergence and Clonal Expansion of in Vitro Artemisinin-Resistant Plasmodium Falciparum Kelch13 R561H Mutant Parasites in Rwanda. *Nat. Med.* 2020, *26* (10), 1602–1608.

(3) Delves, M.; Plouffe, D.; Scheurer, C.; Meister, S.; Wittlin, S.; Winzeler, E. A.; Sinden, R. E.; Leroy, D. The Activities of Current Antimalarial Drugs on the Life Cycle Stages of Plasmodium: A Comparative Study with Human and Rodent Parasites. *PLoS Med.* 2012, *9* (2), e1001169.

(4) Tse, E. G.; Korsik, M.; Todd, M. H. The Past, Present and Future of Anti-Malarial Medicines. *Malar. J.* 2019, *18* (1), 93.

(5) Burrows, J. N.; Duparc, S.; Gutteridge, W. E.; Hooft van Huijsduijnen, R.; Kaszubska, W.; Macintyre, F.; Mazzuri, S.; Möhrle, J. J.; Wells, T. N. C. New Developments in Anti-Malarial Target Candidate and Product Profiles. *Malar. J.* 2017, *16* (1), 26.

(6) Hooft van Huijsduijnen, R.; Wells, T. N. The Antimalarial Pipeline. *Curr. Opin. Pharmacol.*

2018, *42*, 1–6.

(7) Narasimhan, B.; Sharma, D.; Kumar, P. Benzimidazole: A Medicinally Important Heterocyclic Moiety. *Med. Chem. Res.* 2012, *21* (3), 269–283.

(8) Bansal, Y.; Silakari, O. The Therapeutic Journey of Benzimidazoles: A Review. *Bioorg. Med. Chem.* 2012, *20* (21), 6208–6236. https://doi.org/10.1016/j.bmc.2012.09.013.

(9) Salahuddin; Shaharyar, M.; Mazumder, A. Benzimidazoles: A Biologically Active Compounds. *Arab. J. Chem.* 2017, *10*, S157–S173.

(10) Keri, R. S.; Hiremathad, A.; Budagumpi, S.; Nagaraja, B. M. Comprehensive Review in Current Developments of Benzimidazole-Based Medicinal Chemistry. *Chem. Biol. Drug Des.* 2015, *86* (1), 19–65.

(11) Ramachandran, S.; Hameed P., S.; Srivastava, A.; Shanbhag, G.; Morayya, S.; Rautela, N.; Awasthy, D.; Kavanagh, S.; Bharath, S.; Reddy, J.; Panduga, V.; Prabhakar, K. R.; Saralaya, R.; Nanduri, R.; Raichurkar, A.; Menasinakai, S.; Achar, V.; Jiménez-Díaz, M. B.; Martínez, M. S.; Angulo-Barturen, I.; Ferrer, S.; Sanz, L. M.; Gamo, F. J.; Duffy, S.; Avery, V. M.; Waterson, D.; Lee, M. C. S.; Coburn-Flynn, O.; Fidock, D. A.; Iyer, P. S.; Narayanan, S.; Hosagrahara, V.; Sambandamurthy, V. K. N -Aryl-2-Aminobenzimidazoles: Novel, Efficacious, Antimalarial Lead Compounds. *J. Med. Chem.* 2014, *57* (15), 6642–6652.

(12) Chong, C. R.; Chen, X.; Shi, L.; Liu, J. O.; Sullivan, D. J. A Clinical Drug Library Screen Identifies Astemizole as an Antimalarial Agent. *Nat. Chem. Biol.* 2006, *2* (8), 415–416.

(13) Camacho, J.; Barazarte, A.; Gamboa, N.; Rodrigues, J.; Rojas, R.; Vaisberg, A.; Gilman, R.;

Charris, J. Synthesis and Biological Evaluation of Benzimidazole-5-Carbohydrazide Derivatives as Antimalarial, Cytotoxic and Antitubercular Agents. *Bioorg. Med. Chem.* 2011, *19* (6), 2023–2029.

(14) Keurulainen, L.; Vahermo, M.; Puente-Felipe, M.; Sandoval-Izquierdo, E.; Crespo-Fernández, B.; Guijarro-López, L.; Huertas-Valentín, L.; de las Heras-Dueña, L.; Leino, T. O.; Siiskonen, A.; Ballell-Pages, L.; Sanz, L. M.; Castañeda-Casado, P.; Jiménez-Díaz, M. B.; Martínez-Martínez, M. S.; Viera, S.; Kiuru, P.; Calderón, F.; Yli-Kauhaluoma, J. A Developability-Focused Optimization Approach Allows Identification of in Vivo Fast-Acting Antimalarials: N -[3-[(Benzimidazol-2-Yl)Amino]Propyl]Amides. *J. Med. Chem.* 2015, *58* (11), 4573–4580.

(15) Attram, H. D.; Wittlin, S.; Chibale, K. Incorporation of an Intramolecular Hydrogen Bonding Motif in the Side Chain of Antimalarial Benzimidazoles. *Medchemcomm* 2019, *10* (3), 450–455.

(16) Kumar, M.; Okombo, J.; Mambwe, D.; Taylor, D.; Lawrence, N.; Reader, J.; van der Watt, M.; Fontinha, D.; Sanches-Vaz, M.; Bezuidenhout, B. C.; Lauterbach, S. B.; Liebenberg, D.; Birkholtz, L.-M.; Coetzer, T. L.; Prudêncio, M.; Egan, T. J.; Wittlin, S.; Chibale, K. Multistage Antiplasmodium Activity of Astemizole Analogues and Inhibition of Hemozoin Formation as a Contributor to Their Mode of Action. *ACS Infect. Dis.* 2019, *5* (2), 303–315.

(17) Ndakala, A. J.; Gessner, R. K.; Gitari, P. W.; October, N.; White, K. L.; Hudson, A.; Fakorede, F.; Shackleford, D. M.; Kaiser, M.; Yeates, C.; Charman, S. A.; Chibale, K. Antimalarial Pyrido[1,2-a]Benzimidazoles. *J. Med. Chem.* 2011, *54* (13), 4581–4589.

(18) Neftel, K. A.; Woodtly, W.; Schmid, M.; Frick, P. G.; Fehr, J. Amodiaquine Induced Agranulocytosis and Liver Damage. *BMJ* 1986, *292* (6522), 721–723.

(19) Naisbitt, D. J.; Williams, D. P.; O'Neill, P. M.; Maggs, J. L.; Willock, D. J.; Pirmohamed, M.; Park, B. K. Metabolism-Dependent Neutrophil Cytotoxicity of Amodiaquine: A Comparison with Pyronaridine and Related Antimalarial Drugs. *Chem. Res. Toxicol.* 1998, *11* (12), 1586–1595.

(20) Shimizu, S.; Atsumi, R.; Itokawa, K.; Iwasaki, M.; Aoki, T.; Ono, C.; Izumi, T.; Sudo, K.; Okazaki, O. Metabolism-Dependent Hepatotoxicity of Amodiaquine in Glutathione-Depleted Mice. *Arch. Toxicol.* 2009, *83* (7), 701–707.

(21) Birrell, G. W.; Chavchich, M.; Ager, A. L.; Shieh, H.-M.; Heffernan, G. D.; Zhao, W.; Krasucki, P. E.; Saionz, K. W.; Terpinski, J.; Schiehser, G. A.; Jacobus, L. R.; Shanks, G. D.; Jacobus, D. P.; Edstein, M. D. JPC-2997, a New Aminomethylphenol with High In Vitro and In Vivo Antimalarial Activities against Blood Stages of Plasmodium. *Antimicrob. Agents Chemother.* 2015, *59* (1), 170–177.

(22) Peters, W.; Robinson, B. L. The Chemotherapy of Rodent Malaria, XXXVII. *Ann. Trop. Med. Parasitol.* 1984, *78* (6), 561–565.

(23) Powles, M. A.; Allocco, J.; Yeung, L.; Nare, B.; Liberator, P.; Schmatz, D. MK-4815, a Potential New Oral Agent for Treatment of Malaria. *Antimicrob. Agents Chemother.* 2012, *56* (5), 2414–2419.

(24) Reader, J.; Botha, M.; Theron, A.; Lauterbach, S. B.; Rossouw, C.; Engelbrecht, D.; Wepener,

M.; Smit, A.; Leroy, D.; Mancama, D.; Coetzer, T. L.; Birkholtz, L.-M. Nowhere to Hide: Interrogating Different Metabolic Parameters of Plasmodium Falciparum Gametocytes in a Transmission Blocking Drug Discovery Pipeline towards Malaria Elimination. *Malar. J.* 2015, *14*, 213.

(25) Li, X.-Q.; Björkman, A.; Andersson, T. B.; Ridderström, M.; Masimirembwa, C. M. Amodiaquine Clearance and Its Metabolism to N -Desethylamodiaquine Is Mediated by CYP2C8: A New High Affinity and Turnover Enzyme-Specific Probe Substrate. *J. Pharmacol. Exp. Ther.* 2002, *300* (2), 399–407.

(26) Smith, D. A. Evolution of ADME Science: Where Else Can Modeling and Simulation Contribute? *Mol. Pharm.* 2013, *10* (4), 1162–1170.

(27) Varma, M. V. S.; Chang, G.; Lai, Y.; Feng, B.; El-Kattan, A. F.; Litchfield, J.; Goosen, T. C. Physicochemical Property Space of Hepatobiliary Transport and Computational Models for Predicting Rat Biliary Excretion. *Drug Metab. Dispos.* 2012, *40* (8), 1527–1537.

(28) Singh, K.; Okombo, J.; Brunschwig, C.; Ndubi, F.; Barnard, L.; Wilkinson, C.; Njogu, P. M.; Njoroge, M.; Laing, L.; Machado, M.; Prudêncio, M.; Reader, J.; Botha, M.; Nondaba, S.; Birkholtz, L.-M.; Lauterbach, S.; Churchyard, A.; Coetzer, T. L.; Burrows, J. N.; Yeates, C.; Denti, P.; Wiesner, L.; Egan, T. J.; Wittlin, S.; Chibale, K. Antimalarial Pyrido[1,2- a]Benzimidazoles: Lead Optimization, Parasite Life Cycle Stage Profile, Mechanistic Evaluation, Killing Kinetics, and in Vivo Oral Efficacy in a Mouse Model. *J. Med. Chem.* 2017, *60* (4), 1432–1448.

(29) L'abbate, F. P.; Müller, R.; Openshaw, R.; Combrinck, J. M.; de Villiers, K. A.; Hunter, R.;

Egan, T. J. Hemozoin Inhibiting 2-Phenylbenzimidazoles Active against Malaria Parasites. *Eur. J. Med. Chem.* 2018, *159*, 243–254.

(30) Combrinck, J. M.; Mabotha, T. E.; Ncokazi, K. K.; Ambele, M. A.; Taylor, D.; Smith, P. J.; Hoppe, H. C.; Egan, T. J. Insights into the Role of Heme in the Mechanism of Action of Antimalarials. *ACS Chem. Biol.* 2013, *8* (1), 133–137.

(31) Islam, M.; Iskander, M. Microtubulin Binding Sites as Target for Developing Anticancer Agents. *Mini-Reviews Med. Chem.* 2004, *4* (10), 1077–1104.

(32) Bell, A. Microtubule Inhibitors as Potential Antimalarial Agents. *Parasitol. Today* 1998, *14* (6), 234–240.

(33) Parkyn Schneider, M.; Liu, B.; Glock, P.; Suttie, A.; McHugh, E.; Andrew, D.; Batinovic, S.; Williamson, N.; Hanssen, E.; McMillan, P.; Hliscs, M.; Tilley, L.; Dixon, M. W. A. Disrupting Assembly of the Inner Membrane Complex Blocks Plasmodium Falciparum Sexual Stage Development. *PLOS Pathog.* 2017, *13* (10), e1006659.

(34) Kappes, B.; Rohrbach, P. Microtubule Inhibitors as a Potential Treatment for Malaria. *Future Microbiol.* 2007, *2* (4), 409–423.

(35) Spreng, B.; Fleckenstein, H.; Kübler, P.; Di Biagio, C.; Benz, M.; Patra, P.; Schwarz, U. S.; Cyrklaff, M.; Frischknecht, F. Microtubule Number and Length Determine Cellular Shape and Function in Plasmodium. *EMBO J.* 2019, *38* (15), e100984.

(36) Sinden, R. E.; Smalley, M. E. Gametocytogenesis of Plasmodium Falciparum in Vitro : The Cell-Cycle. *Parasitology* 1979, *79* (2), 277–296.

(37) Sinden, R. E.; Hartley, R. H.; King, N. J. Gametogenesis in Plasmodium; The Inhibitory Effects of Anticytoskeletal Agents. *Int. J. Parasitol.* 1985, *15* (2), 211–217.

(38) Snyder, C.; Chollet, J.; Santo-Tomas, J.; Scheurer, C.; Wittlin, S. In Vitro and in Vivo Interaction of Synthetic Peroxide RBx11160 (OZ277) with Piperaquine in Plasmodium Models. *Exp. Parasitol.* 2007, *115* (3), 296–300.

(39) González Cabrera, D.; Douelle, F.; Younis, Y.; Feng, T.-S.; Le Manach, C.; Nchinda, A. T.; Street, L. J.; Scheurer, C.; Kamber, J.; White, K. L.; Montagnat, O. D.; Ryan, E.; Katneni, K.; Zabiulla, K. M.; Joseph, J. T.; Bashyam, S.; Waterson, D.; Witty, M. J.; Charman, S. A.; Wittlin, S.; Chibale, K. Structure–Activity Relationship Studies of Orally Active Antimalarial 3,5-Substituted 2-Aminopyridines. *J. Med. Chem.* 2012, *55* (24), 11022–11030.

(40) Reader, J.; Botha, M.; Theron, A.; Lauterbach, S. B.; Rossouw, C.; Engelbrecht, D.; Wepener, M.; Smit, A.; Leroy, D.; Mancama, D.; Coetzer, T. L.; Birkholtz, L.-M. Nowhere to Hide: Interrogating Different Metabolic Parameters of Plasmodium Falciparum Gametocytes in a Transmission Blocking Drug Discovery Pipeline towards Malaria Elimination. *Malar. J.* 2015, *14* (1), 213.

(41) Coetzee, N.; von Grüning, H.; Opperman, D.; van der Watt, M.; Reader, J.; Birkholtz, L.-M. Epigenetic Inhibitors Target Multiple Stages of Plasmodium Falciparum Parasites. *Sci. Rep.* 2020, *10* (1), 2355.

(42) Mosmann, T. Rapid Colorimetric Assay for Cellular Growth and Survival: Application to Proliferation and Cytotoxicity Assays. *J. Immunol. Methods* 1983, *65* (1–2), 55–63.

(43) Verlinden, B. K.; Niemand, J.; Snyman, J.; Sharma, S. K.; Beattie, R. J.; Woster, P. M.; Birkholtz, L.-M. Discovery of Novel Alkylated (Bis)Urea and (Bis)Thiourea Polyamine Analogues with Potent Antimalarial Activities. *J. Med. Chem.* 2011, *54* (19), 6624–6633.

(44) Di, L.; Kerns, E. H.; Gao, N.; Li, S. Q.; Huang, Y.; Bourassa, J. L.; Huryn, D. M. Experimental Design on Single-Time-Point High-Throughput Microsomal Stability Assay. *J. Pharm. Sci.* 2004, *93* (6), 1537–1544.

(45) Zhou, L.; Yang, L.; Tilton, S.; Wang, J. Development of a High Throughput Equilibrium Solubility Assay Using Miniaturized Shake-flask Method in Early Drug Discovery. *J. Pharm. Sci.* 2007, *96* (11), 3052–3071.

(46) Kerns, E. H.; Di, L. *Preface*; 2008.

(47) Wohnsland, F.; Faller, B. High-Throughput Permeability PH Profile and High-Throughput Alkane/Water Log P with Artificial Membranes. *J. Med. Chem.* 2001, *44* (6), 923–930.

(48) Faller, B. Artificial Membrane Assays to Assess Permeability. *Curr. Drug Metab.* 2008, *9* (9), 886–892.

(49) Combrinck, J. M.; Fong, K. Y.; Gibhard, L.; Smith, P. J.; Wright, D. W.; Egan, T. J. Optimization of a Multi-Well Colorimetric Assay to Determine Haem Species in Plasmodium Falciparum in the Presence of Anti-Malarials. *Malar. J.* 2015, *14* (1), 253.

TABLE OF CONTENTS GRAPHIC

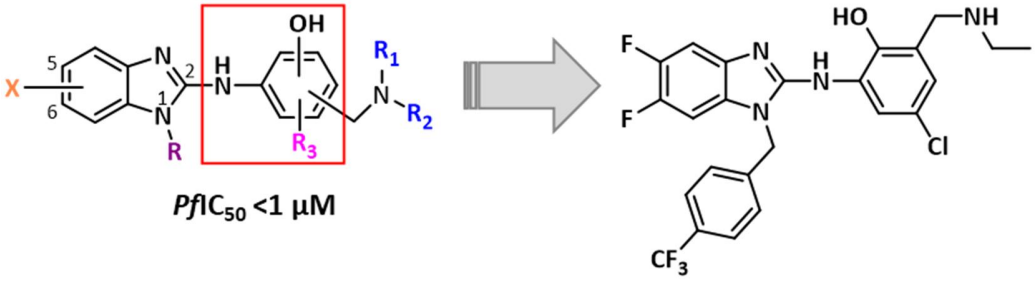

*Pf*IC$_{50}$ <1 µM

P. berghei, *in vivo* studies
(**41**, p.o. 98% activity, F = 24%)